CHALMERS
UNIVERSITY OF TECHNOLOGY

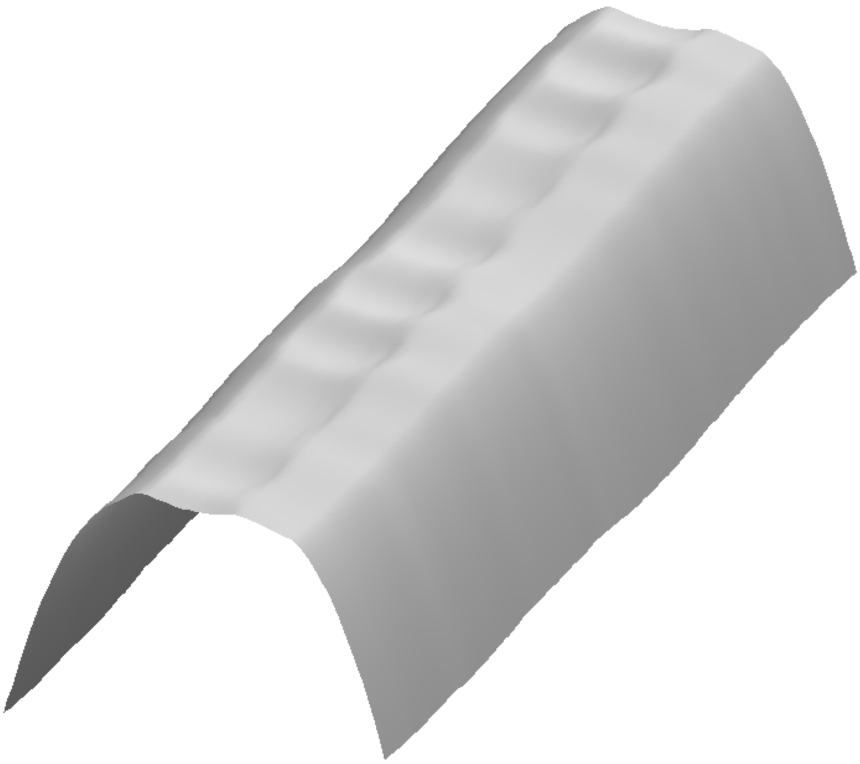

Simulation of Rail Corrugation Growth on Curves

Master's thesis in Applied Mechanics

ANDREAS CARLBERGER

Department of Applied Mechanics, Division of Dynamics
CHALMERS UNIVERSITY OF TECHNOLOGY
Gothenburg, Sweden 2016

Master's thesis 2016:59

Simulation of Rail Corrugation Growth on Curves

Simulation of Dynamic Vehicle–Track Interaction by using a Multibody Dynamics Software and Prediction of Corrugation Growth on Small Radius Curves

ANDREAS CARLBERGER

CHALMERS
UNIVERSITY OF TECHNOLOGY

Department of Applied Mechanics
Division of Dynamics
Chalmers University of Technology
Gothenburg, Sweden 2016

Simulation of Rail Corrugation Growth on Curves

ANDREAS CARLBERGER

Supervisors:
Peter Torstensson, Department of Applied Mechanics, Chalmers.
Anders Frid, ÅF Industry.
Examiner:
Jens Nielsen, Department of Applied Mechanics, Chalmers.

Master's Thesis 2016:59
ISSN 1652–8557
Department of Applied Mechanics
Division of Dynamics
Chalmers University of Technology
SE-412 96 Gothenburg
Telephone +46 31 722 1000

Cover: Matlab visualization of predicted corrugation showing a section of the rail crown.

Typeset in LaTeX
Printed by Chalmers Reproservice
Gothenburg, Sweden 2016

Simulation of Rail Corrugation Growth on Curves
ANDREAS CARLBERGER
Department of Applied Mechanics
Chalmers University of Technology

Abstract

Rail corrugation (periodic surface irregularities at distinct wavelengths) is a problem experienced by many railway networks worldwide. Corrugation induces a pronounced dynamic wheel–rail contact loading that leads to increased generation of noise and in severe cases even damage of vehicle and track components. The large magnitude creep forces and sliding between wheel and rail make corrugation especially prone to develop on curves. The current work summarizes the results from a Master Thesis project performed in collaboration between Chalmers, ÅF Industry, Bombardier Transportation and Stockholm Public Transport.
A time-domain model for the prediction of long-term growth of rail roughness has been developed. Dynamic vehicle–track interaction in a broad frequency range (at least up to 300 Hz) is simulated using the commercial software SIMPACK. Wheelset structural flexibility is accounted for by using modal parameters calculated with a finite element model. Non-Hertzian and non-steady wheel–rail contact and associated generation of wear are calculated in a post-processing step in the software Matlab. Archard's law is applied to model the sliding wear. A large number of train passages is accounted for by recurrent updating of the rail surface irregularity based on the calculated wear depth.
The proposed prediction model is applied to investigate a curve on the Stockholm metro network exposed to severe corrugation growth. The predictions show corrugation growth to be generated by the leading wheelset of passing bogies at wavelengths approximately corresponding to those observed on the reference curve of the Stockholm metro. The corrugation wavelengths are related to coupled vibrations of the vehicle–track system involving wheelset bending eigenmodes. The influence of the wheelset structural flexibility and wheel–rail contact friction on corrugation growth is investigated.

Keywords: Rutting corrugation, non-Hertzian and non-steady wheel–rail contact, roughness growth prediction, wavelength fixing mechanism, small radius curves, multibody dynamics, Simpack.

Acknowledgements

This thesis is written by me, Andreas Carlberger, as part of my Master's studies in Applied Mechanics at Chalmers University of Technology. The work was carried out during the first half of 2016 at Chalmers in cooperation with ÅF Industry, Bombardier Transportation and SLL (Stockholm Public Transportation).
I would like to thank Dr Babette Dirks, Dr Rickard Nilsson and Dr Björn Pålsson for giving their expert input on a regular basis. I thank my supervisor and future boss, Dr Anders Frid for valuable inputs and many interesting discussions. I am very grateful for the extensive support form my primary supervisor, Dr Peter Torstensson, who has given excellent guidance throughout the project. Docent Jens Nielsen is acknowledged for professional inputs and feedback.
I want to thank my family and friends for supporting me and being there. Most of all I am grateful to you, Annie. Without you I would not have done this thesis and I have enjoyed this time mostly because of you.

Andreas Carlberger, Gothenburg, July 2016

Contents

List of Figures

1
Introduction

1.1 Background

In today's modern cities the metro is one of the most environmentally friendly and effective modes of transportation. The metro often operates in narrow spaces and in densely populated areas. This puts requirements on limited noise emission and adaptability to geometric restrictions.
Many recurrent problems with railway vehicles are associated with curving. During curving high magnitude normal and tangential forces are generated in the wheel–rail contacts leading to damage and noise. The damage occurs on both wheels and rails as rolling contact fatigue and wear.
A particular prominent problem is the development of periodic irregularities with distinct wavelengths on the crown of the low rail in curves. This phenomenon, referred to as "rutting" corrugation, has been explained by wear generated at certain wavelengths. The corrugation wavelength developed at a specific site is determined by the complex vehicle–track interaction. In particular, eigenmodes of the wheelset in bending and torsion have often been pointed out as the root cause.
Observations of this kind of corrugation are reported from several metro track networks worldwide. Currently the most common mitigation action is recurring rail grinding but this is costly and does not prevent the formation of new irregularities.

1.2 Purpose

The aim of this project is to develop a model for accurate prediction of rail corrugation growth on curves. By use of numerical modelling the complex conditions that promote corrugation growth can be identified. In particular, such a model could be applied to investigate the potential of finding a design solution to the problem or to set limits for operating conditions. The optimization and planning of track maintenance by infrastructure managers are other areas where this model can be shown to be useful.

1.3 Limitations

The model is developed to mimic the dynamic interaction between a Bombardier C20 train and a specific curve on the Stockholm metro. The frequency range below

250 Hz is studied. This is sufficient to capture the excitation frequencies corresponding to the dominant corrugation wavelengths observed on the reference curve. High–frequency curve squeal is not assessed in the current work.
In principle the proposed modelling framework is generally applicable to investigate causes of rail roughness growth provided that the dynamic behaviour of the vehicle–track system in the studied frequency range is accounted for.
The simplified vehicle model includes only one car of which only the first bogie is used to predict rail wear. Only corrugation growth on the low rail is considered.
No driving torque was applied to the wheelsets. Only nominal wheel and rail profiles are used.

2 Theory

2.1 Review of numerical prediction of corrugation growth on small radius curves

In the doctoral thesis of P.T. Torstensson [1] rutting corrugation on small radius curves is studied. It considers the same reference curve as the present thesis. The specific type of corrugation called rutting on the low rail is both analyzed through field measurements and modelled using a numerical time-domain vehicle–track model. On the reference curve, rutting corrugation with wavelengths 5 cm and 8 cm are linked to vibrations of the leading wheelsets of passing bogies in their first and second bending eigenmodes. The developed time-domain model uses a non-Hertzian and non-steady wheel–rail contact model. The model was validated in the frequency range below approximately 250 Hz. Predictions showed a large dependence of the friction on the development of corrugation. For friction below 0.3 almost no corrugation growth was predicted. This is in agreement with results from field tests where a friction modifier was applied on the reference curve. Furthermore it was predicted and confirmed by observation that the corrugation develops towards a constant amplitude. This phenomenon was attributed to a decreasing phase difference between the calculated wear and the accumulated rail irregularity. In a metallurgic study plastic deformation on the rail crown towards the field side was found, indicating large magnitude lateral creepages in the curve.

In an article by Knothe and Groß-Thebing [2] short pitch corrugation and the influence of contact mechanics is discussed. It was found that the vehicle–track dynamic behaviour promotes corrugation growth in the interval between 2 cm and 10 cm. The contact mechanics were identified to play an important role in the formation of short wavelength rail corrugation. The non-steady-state contact mechanics are strongly linked to the wavelength fixing mechanisms. The structural dynamics of the track was found to have significant influence of the wear process. Lateral vibration of the rail together with lateral creepage in the contact yields transient creepage fluctuations. These fluctuations are associated with the development of corrugation. The currently most effective mitigation of corrugation is rail grinding. The large magnitude wheel–rail contact forces may cause stresses large enough to produce plastic flow in the top of the rail surface. The resulting residual stresses will be periodic with the corrugation and also have to be removed during grinding. It is therefore not enough to only remove the geometric irregularity.

The Influence of wheelset and track structural flexibility on the dynamic interaction was investigated by Chaar [3]. The work included both simulations and measurements. It was found that the structural flexibility of the wheelset and track significantly influences the wheel–rail contact forces. A set of parametric studies showed that simulations of wheel–rail contact forces can be significantly improved if the track receptance is represented accurately.

2.2 The vehicle–track system

In the following a brief introduction to general railway theory and railway concepts is given. A more comprehensive summary can be found in the text books Rail Vehicle Dynamics [4] or Modern Railway Track [5].

Rails provide a load bearing running surface with high geometric tolerances. Due to the large, local and cyclic loads from passing wheels high demands are set on their mechanical properties such as hardness, strength, toughness, wear resistance and fatigue strength. The metal should also not become brittle at low temperatures. The rails are mounted to the sleepers with a stiff fastener. Sleepers are normally spaced with about 60 cm. A plastic or rubber pad separates the rail and sleeper and provides resilience and damping. The sleepers are laid on ballast that consist of crushed stone.

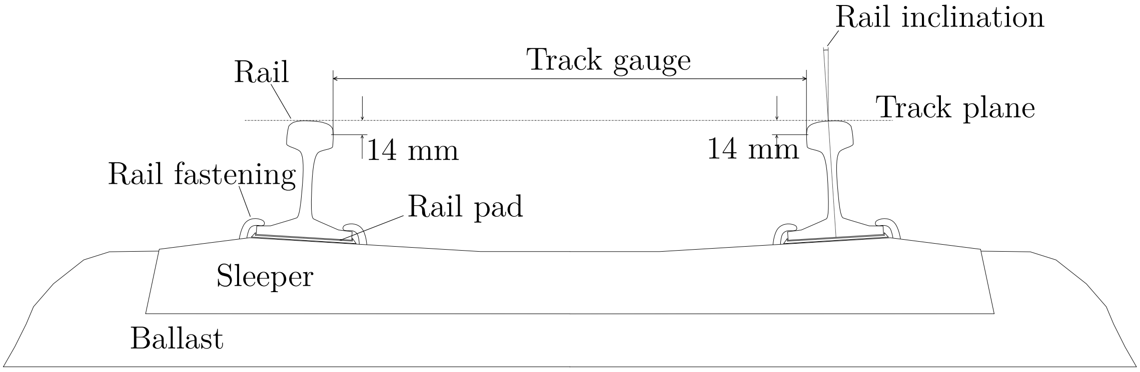

Figure 2.1: Track cross section and important components.

Railway curves consist of a transition curve and a circular curve. Transition curves connecting tangent track and circular curves have a continuous varying curvature which limits the lateral change of acceleration for passing trains.
The definition of some track components is shown in Figure 2.1. Track gauge is a measure of the distance between the rails. The measuring point is defined as the point closest to the other rail at no more than 14 mm from the top of the rail vertically in the track coordinate system. To counteract the effects of the centrifugal accelerations of passing trains, curved track are constructed with a angle with respect to the horizontal plane. This is called superelevation or cant. Often the rails are mounted at an angle with respect to the track plane. This is called inclination and results in a enlarged contact area between the wheel and rail, and a better

transmission of forces between the rail and sleeper. The inclination is typically between 1:40 and 1:20 (in Sweden 1:30).

2.2.1 Irregularities

A distinction is often made between long and short wavelength irregularities. Irregularities on the rail top with wavelengths below 20 cm are denoted “rail roughness”. These are present at varying amplitudes and the cause can for example be rail grinding or irregular wear caused by passing trains. The initial irregularity is essential for the development of new irregularities [2].

Deviations of the rail location from the design geometry can be denoted as “track irregularities” and are quantified by measurements of vertical displacement, lateral displacement, gauge and cant. The wavelengths are typically ranging from 20 cm to 25 m. These track irregularities have a significant influence on the low frequency dynamic behaviour of the train [4].

In the current work only the first type of irregularity is considered.

2.2.2 Vehicle

Conventionally train cars are supported by two bogies. In some cases two cars can share a bogie. The car is mounted to the bogie via the secondary suspension. A bogie is a frame normally holding two wheelsets. The connection between them is called the primary suspension. Wheelsets consist of two wheels rigidly connected by a wheelaxle. The mounting of the primary suspension is on the outside of the wheels. On many modern trains all wheelsets are driven. The torque is applied to a sprocket on the wheel axle. An illustration containing the most basic train components can be seen in Figure 2.2a.

2.2.3 Steering of rail vehicles

The wheel profile consists of a wheel tread and a wheel flange. In normal conditions only the tread is in contact with the rail. The wheel flange restricts the wheelset movement in the lateral direction. The conicity of the tread gives the wheel different effective rolling radii depending on the lateral contact position, see Figure 2.2b. By having different effective radius on its wheels, a rolling wheelset will steer towards the wheel with smaller radii and therefore reduces the risk of flange contact. Due to the conicity of the wheels the wheelset will automatically steer towards the centre of the track. This explains why curving without flange contact is possible. Flange contact is generally associated with large magnitude forces in combination with excessive wear and should therefore be avoided to the largest extent. The effective radii are determined by the wheelset position and the rail and wheel profiles. The track gauge is often widened in curves to reduce the likelihood of flange contact and to allow larger running radius difference of the two wheels.

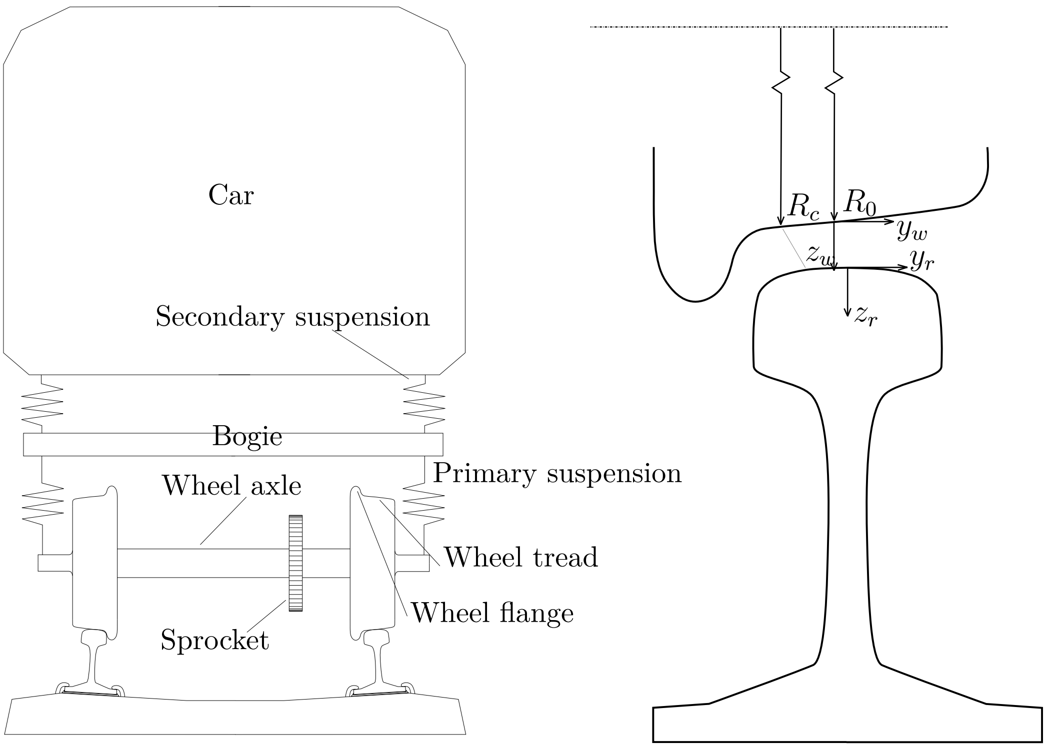

(a) **(b)**

Figure 2.2: (a), Main vehicle components. (b), Wheel and rail profiles and definition of coordinate systems.

2.3 Simulation of dynamic vehicle–track interaction

The wheel-rail contact forces are in the low-frequency range due to car body steering and in the high-frequency range up to about 2000 Hz caused by irregularities in the wheel–rail contact. In the following important concepts for the simulation of dynamic vehicle-track interaction are introduced.

2.3.1 Mathematical formulation

The system of equations describing the dynamic vehicle-track interaction can be analyzed in the frequency- or time-domain. The non-linear system of equations can be written as

$$\mathbf{M}\ddot{\mathbf{u}} + \mathbf{C}\dot{\mathbf{u}} + \mathbf{K}\mathbf{u} = \mathbf{Q} \tag{2.1}$$

M, **C** and **K** are the mass, damping and stiffness matrices. **Q** constitutes external forces and **u** holds state variables such as displacements, rotations and modal displacements. These equations may be complemented with a set of constraint equations. Analysis in the frequency domain is based on a linearization at a specific state. This can give valuable information about the behaviour of the model. However, to capture transients and non-linearities, a time-domain model is required. Solution is typically obtained through computationally demanding numerical integration.

2.3.2 Track

The frequencies of the rail–wheel contact forces range from a few Hz related to car body motions up to more than 2000 Hz related to irregularities in the wheel–rail contact. To correctly assess the magnitudes of the corresponding forces the dynamics of the track in the same frequency range needs to be modelled. Depending on the analysis, different ranges of frequencies need to be accounted for and the track model should be chosen accordingly.

2.3.2.1 Continuous track models

A common way of accounting for the track dynamics is to model a section of the track with high resolution using the finite element (FE) method. The number of degrees-of-freedom (dofs) of the track model can be reduced through modal superposition retaining only a truncated set of low frequency eigenmodes. Some methods [6, 7, 8] model the rails by using beam theory and the other components with mass-spring-damper systems.

2.3.2.2 Moving track models

Often in simulations of dynamic vehicle-track interaction a so-called moving track model, corresponding to a simple representation of the track following each wheelset, is applied. This allows for much longer simulation distances as the model size is independent of the track length. In this method longitudinal dynamics and interaction of wheels through the track are disregarded. Typically the track is represented by a mass-spring-damper system. In principle the properties of this mechanical system can be varied periodically to account for the discrete sleeper support.

2.3.3 Vehicle

The basic components included in a vehicle model were presented in Section 2.2.2. Often significant simplifying assumptions are used. The secondary suspension connecting the bogie to the car contains airsprings, antirollbars and yaw dampers making up a complex non-linear six-dof connection. In modelling this system is typically linearized.

The structural flexibility of vehicle components is typically accounted for by the FE method. However these representations generally include a large number of dofs and hence they are computationally demanding. To reduce the computational cost some vehicle components may be modelled as rigid. In studies that focus on high-frequency wheel–rail contact forces, the wheelsets are also commonly modelled as flexible. The representation of the flexible bodies normally only contain a small set of its lowest frequency eigenmodes.

2.3.4 Wheel–rail contact

For a given state of the rail and wheel in the time-integration of dynamic vehicle-track interaction, the normal and tangential forces in the wheel-rail contact need to be accurately calculated. Moreover for calculating the wear generated on the wheel or rail not only forces and slip velocities need to be known, but also their respective distribution within the contact patch. The high stiffness and the non-linear force-displacement relation in the wheel-rail contact puts requirements on using a high sampling frequency in the time-integration procedure. In order to reduce the computational effort simplifying assumptions need to be made. In this section the basic theory and two of the most popular methods are briefly presented. A full introduction to the theory of contact mechanics can be found in the work of Johnson [9]. More about the current research in the field of wheel–rail contact can be found in the thesis of Sichani [10].

2.3.4.1 Rolling contact mechanics

The wheelset curving behaviour discussed in Section 2.2.3 assumes that the contact exists in one point and that no sliding is present, i.e. pure rolling. Due to elasticity, the contact is in reality made over a small contact patch. Also a portion of the contact area may be sliding. Carter [11] presented that in order for a rolling contact to yield a tangential force a velocity difference between the contacting bodies needs to be present. This velocity difference is called creepage and is due to both elastic deformation of the two bodies and slip in the rear of the contact patch. The creepage is defined as

$$\gamma = \frac{v_w - v_r}{v_{ref}} \tag{2.2}$$

where v_w and v_r are the velocities in the contact point with respect to an inertial coordinate system for the wheel and rail, respectively. v_{ref} is a reference velocity normally taken as the vehicle speed. The creepage can be calculated in both longitudinal and lateral directions, as well as with respect to the angular velocity difference, then called spin.

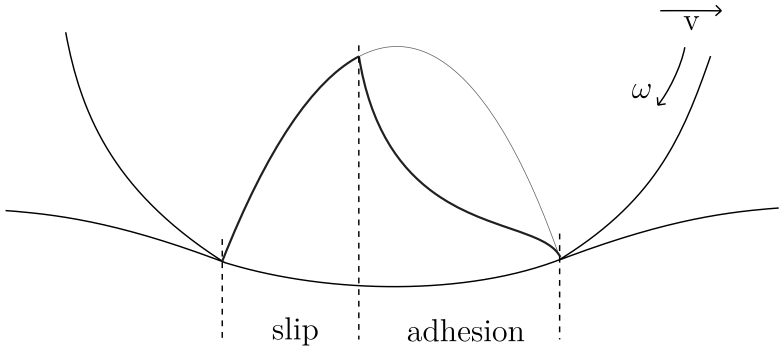

Figure 2.3: Illustration of contact of rolling cylinder on halfspace. Distribution of normal force (thin line). Distribution of tangential force (thick line).

All rolling contacts that transmit a tangential force have a region of slip in the wheel–rail contact area. This region increases from the rear towards the front of the wheel–rail contact area with increasing creepage. The shear force distribution is illustrated in Figure 2.3 for a cylinder rolling on an elastic halfspace. The shear force can be modelled using the well known Coulomb's friction model

$$T \begin{cases} \leq & \mu F, \quad \text{if adhesion} \\ = & \mu F, \quad \text{if slip} \end{cases} \tag{2.3}$$

which gives the tangential force in a point as the smallest force that prevents sliding until the limit μF is reached. It therefore defines the region of slip and adhesion. Generally the friction is significantly lower for sliding contact but this is often neglected in models of wheel–rail contact.

2.3.4.2 Common assumptions

The elastic halfspace assumption is widely used in the field of contact mechanics [9]. It implies that the contacting bodies are non-conformal and that the dimensions of the contact area are significantly smaller than the local radii of the contacting bodies. According to this assumption, the bodies can be regarded as flat semi-infinite elastic solids in the calculation of internal stresses and deflections. Influence functions describing the behaviour of an arbitrary surface can then be calculated based on the work of Boussinesq [12] and Cerruti [13]. Assuming that the bodies are quasi-identical, for a given pressure distribution p, the surface displacement in the normal direction is given as

$$u(x, y) = \frac{1-\nu^2}{\pi E} \iint_A \frac{p(\xi, \eta)}{\sqrt{(x-\xi)^2 + (y-\eta)^2}} \mathrm{d}\xi \mathrm{d}\eta \tag{2.4}$$

where ν and E are the Poisson's ratio and the modulus of elasticity, respectively. If the two contacting bodies have the same elastic constants or

$$\frac{G_1}{1-2\nu_1} = \frac{G_2}{1-2\nu_2}, \tag{2.5}$$

where G and ν are the shear modulus and Poisson's ratio for the two bodies, the bodies are said to be quasi-identical. This implies that the bodies will deform identically when pressed together and the contact plane will remain flat. If the contact is non-conformal this will lead to the normal and tangential contact problems being uncoupled.

2.3.4.3 Hertzian contact

Hertz [14] developed an efficient theory for the elastic contact between two bodies. The theory is based on the following set of assumptions; the contact area is small compared to the size of the contacting bodies, the curvature of the bodies are close to constant in the vicinity of the contact patch and friction is negligible. The last assumption is needed to uncouple the normal and tangential contact problems and can therefore be disregarded if the bodies are close to quasi-identical. Defining a coordinate system with origin in the point where the bodies first touch and the z-axis normal to the contact surface, each body can be approximated using a quadratic function as

$$z_i = A_i x^2 + B_i y^2 + C_i xy \tag{2.6}$$

The rotation of the coordinate system can be set such that the distance between the undeformed bodies $h = z_1 - z_2$ becomes a function of two terms

$$h = Ax^2 + By^2, \tag{2.7}$$

$$A = \frac{1}{2R'_e} = \frac{1}{2R'_1} + \frac{1}{2R'_2}, \quad B = \frac{1}{2R''_e} = \frac{1}{2R''_1} + \frac{1}{2R''_2}. \tag{2.8}$$

Here R denotes the radii of curvature in both directions. The superscript R' and R'' denote major and minor relative radius respectively. R_e denotes the equivalent radii.
Using the halfspace assumption the distribution of normal contact pressure is obtained as

$$p = p_0\sqrt{1 - (x/a)^2 - (y/b)^2} \tag{2.9}$$

where p_0 is the maximum pressure at the centre of the contact, and a and b are the contact semi-axes. The total normal force then becomes

$$P = \frac{2}{3} p_0 \pi ab \tag{2.10}$$

2.3.4.4 Kalker's variational method

In many cases of rolling contact the curvature of the geometries in contact varies significantly in the contact patch. In these cases the Hertz assumption may be too crude. Kalker's variational method can account for these conditions and is based on his non-steady and non-linear theory of rolling contact [15], often referred to as Kalker's complete theory. The contacting geometries are discretized locally in the vicinity of the contact. The elastic deformation of the contacting bodies is calculated using the boundary element method and the Boussinesq-Cerruti integral in Equation 2.4. The rolling contact problem is solved in its weak form. Often quasi-identity is assumed resulting in a separation of the normal and tangential contact problems. This algorithm is often used as a reference solution as it converges to the exact solution for any set of geometries that fulfil the halfspace assumption. Another advantage is that it allows for the modelling of transient effects in the wheel–rail contact. According to Knothe and Groß-Thebing [2] this is necessary if the contact patch is larger than 1/10 of the studied corrugation wavelength. This is often the case on corrugated rail.

2.4 Wear model

Archard's wear model [16] is based on the assumption that the volume of removed material is proportional to the dissipated energy. The dissipation of energy is the work done by frictional forces so wear is only present in the sliding part of the contact. This model is derived using the theory of asperity contact and was first done by Reye in 1860 [17]. The Archard equation for the wear volume is as follows

$$V_{wear} = k\frac{Ns}{H} \tag{2.11}$$

The wear volume is proportional to both the normal force, N, and the sliding distance, s. H is the hardness constant of the softer material and k is a wear constant normally ranging from 10^{-8} to 10^{-2}. The magnitude of the loading, the material and the local friction are typically the factors influencing k. Empirically this dependence has been found and tabulated for wheel and rail materials, varying creepage and N/H ratios, by Jendel [18]. In combination with a discrete contact model it can be useful to re-write Equation 2.11 as

$$\Delta z_{wear}(x,y) = k\frac{p(x,y)\gamma(x,y)\mathrm{d}x}{H} \tag{2.12}$$

where Δz is the local wear depth, p is the pressure, γ is the total local creepage and $\mathrm{d}x$ is the element length.

3
Method

Although the strategy developed in this thesis is a general approach to predict wear and corrugation, it is used for a specific curve on the Stockholm metro. This reference curve is trafficked exclusively by Bombardier's metro train C20.
The basis for the prediction of corrugation growth can be split in two major parts; the simulation of dynamic vehicle–track interaction and the generation of wear on the rails. By accurate modelling of both in the frequency range of interest, the mechanisms causing corrugation may be found.
In several studies eigenmodes of the unsprung mass, i.e. the wheelset, have been associated with the development of different types of rail corrugation [19]. In the current work the wheel axle is modelled as flexible.
In the following the foundation for the simulation model and its configuration is presented.

3.1 Reference curve

A curve in the Stockholm metro exposed to severe corrugation growth on the low rail is used as a reference. The prediction model is developed to resemble the conditions in this curve.
The track layout of interest consists of a curve with a radius of 120 m. The curve is preceded by a straight (tangent) track section and a 50 m long transition curve. The transition curve is an Euler clothoid, a spiral with linearly varying curvature. The track cant also increases linearly over the transition curve from zero on the straight track to 9 cm in the curve. A constant gauge of 1435 mm is used throughout this section. Rails are inclined towards the centre of the track with angle 1:40. BV50 rails and S1002 wheel profiles are used.
The traffic on the curve consists exclusively of the C20 train manufactured by Bombardier Transportation. The speed of passing trains in the specified curve is approximately 30 km/h. The curve has previously been subjected to two measurement campaigns. The measurements have included track receptance, rail irregularity and noise from passing trains. The first campaign performed in 2008, initially presented by Torstensson et al. [20], shows distinctive corrugation growth at the wavelengths of 4.5 and 8 cm. For a vehicle speed of 30 km/h, this corresponds to excitation frequencies of about 185 Hz and 104 Hz. It was also noted that the corrugation amplitude at the corresponding wavelengths approach a constant value after less than one year after rail grinding. The noise data is strongly dominated by frequencies significantly higher than those associated with the rail corrugation. Results from

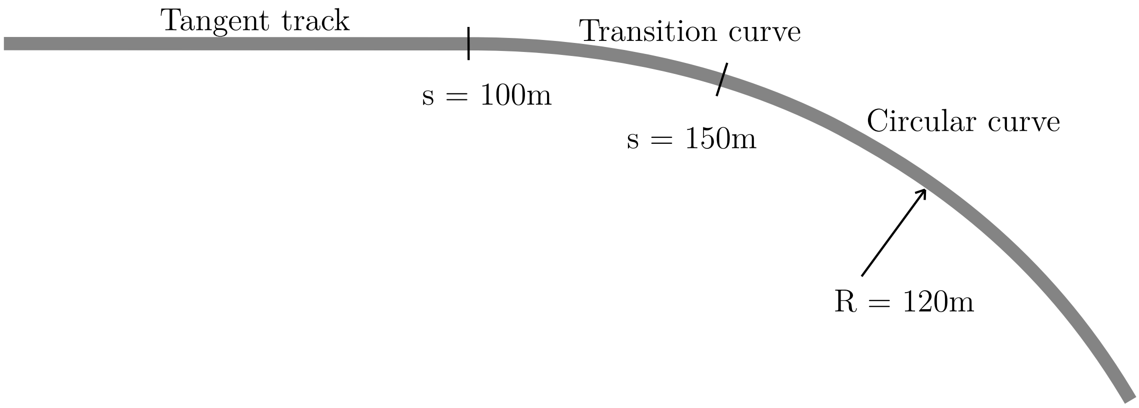

Figure 3.1: Curve layout.

another measurement done in 2015 is described in Section 4.1.

3.2 Model in Simpack

Simpack is a commercial software for dynamic simulation of mechanical multibody systems (MBS). It's module Simpack Rail has become one of the most used MBS-software tools for simulating railway vehicle dynamics. The Simpack pre-processor enables setup of a model by usage of simple elements such as rigid bodies, springs, dampers, constraints and joints. More advanced components such as flexible bodies and wheel–rail contacts can also be used. Specifically, the wheel–rail contact element takes care of everything concerning the contact such as contact detection, normal and tangential force distribution and creep velocities. It can also handle multiple contact points per wheel–rail pair. The structural flexibility of bodies in the mechanical system needs to be accounted for through input from other FE-software. The equations of motion set up by Simpack's pre-processor are integrated using solver SODASRT 2 [21]. In Simpack, the equations of motion and the corresponding structural element matrices can not be exported to an output file.
An effective way of reducing the simulation time is to use a so called continuation run. This type of simulation is based on the end states of a prior simulation and enables different continuations on a simulation as long as the transition between the two is smooth. This feature was used in the current work to continue simulations in the circular curve. This way, simulations on the tangent track and the reference curve did not have to be re-run.

3.2.1 Track

A moving track model was used to represent the dynamics of the track. Here the chosen model consists of a representation of the rails, sleeper, rail fastening, ballast and rail pads. A schematic picture of the wheelset and track can be seen in Figure 3.2. The rail stiffness is accounted for by using an added undamped connection directly to the ground. A similar model was made in [22] where the rail stiffness

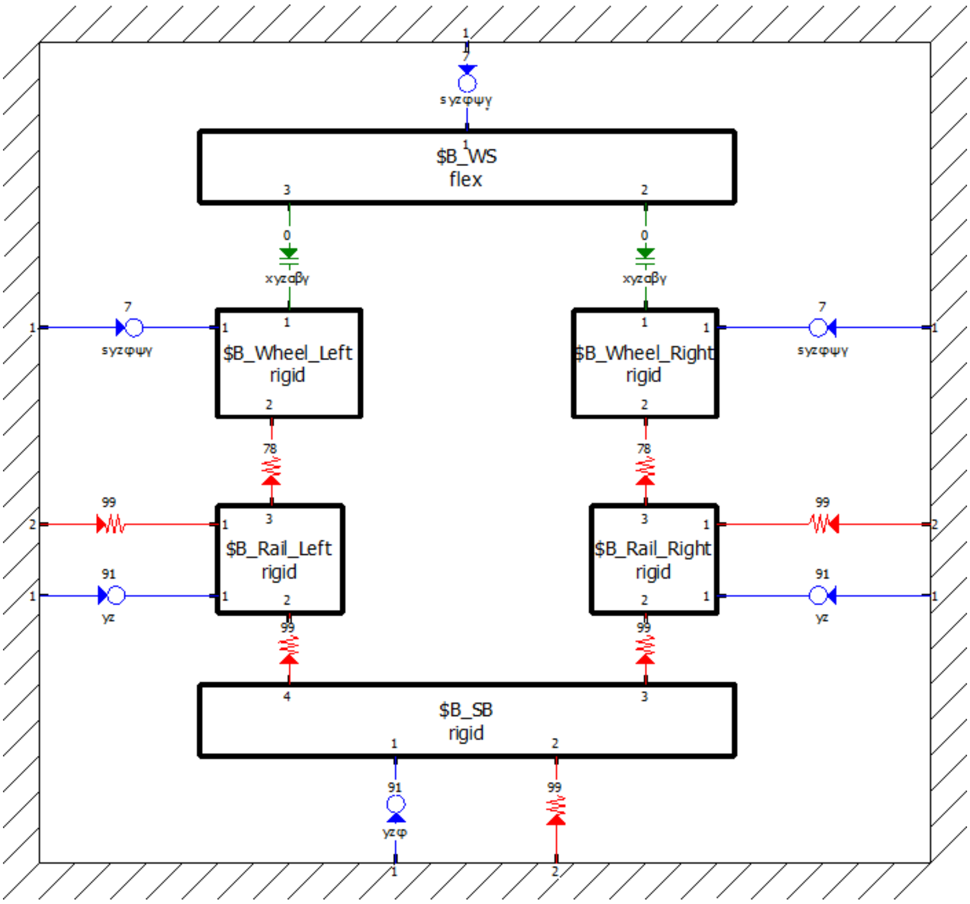

Figure 3.2: Flexible wheelset and track model in Simpack. The bodies respective degrees of freedom are noted under the circle/arrow joint symbols (blue). The spring/arrow symbols (red) denote spring and damper connections and the bars/arrow symbols (green) denote constraints.

was accounted for by adopting a Guyan-Irons reduction on an Euler-Bernoulli-Saint-Venant beam representing the rail.

An important property of the track is its resulting displacement amplitude due to a sinusoidal unit load. This quantity is called receptance. In field, the receptance can be measured in a sledge hammer test [20]. The rail is impacted with a sledge hammer equipped with a load cell and the resulting displacement in the rail is measured with an accelerometer. Both lateral and vertical receptance are assessed. Measurements were performed above a sleeper as well as in the middle of a sleeper span. Using this data a linear response has to be assumed.

The track properties are calibrated towards field test data though optimization with respect to the receptance magnitude and phase in both lateral and vertical directions. The frequency range between 50 Hz and 600 Hz is considered. For this a particle swarm optimization was used, starting from estimated parameters for the properties. The calculated and measured track receptances are compared in Figure 3.3.

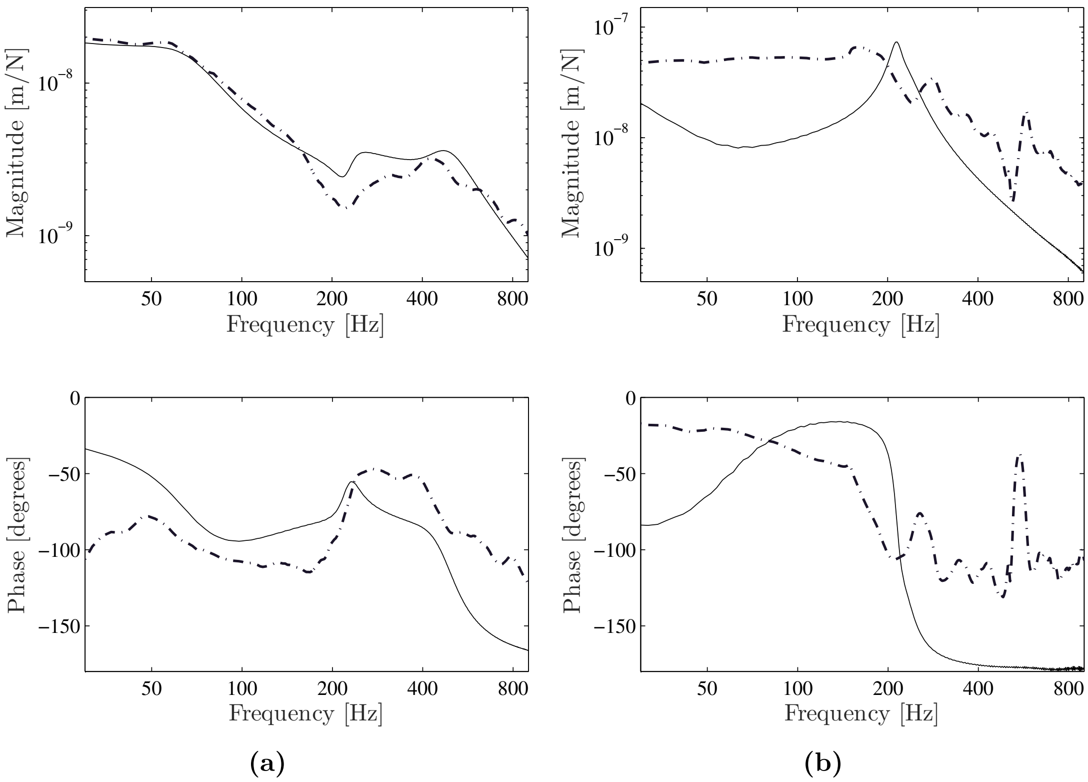

Figure 3.3: Track direct receptance in vertical (a) and lateral (b) directions: calculated (—) and measured (-·-).

3.2.2 Vehicle

A C20 train is formed by three units coupled together. A unit is 47m and consists of three inseparable car bodies. The two end cars are hinged to the middle car by a semi-trailer arrangement, thereby reducing the number of bogies from six to four.

The train model was obtained from Bombardier Transportation. In order to reduce simulation time, a vehicle model consisting of only one car is used. The two bogies of the car were adjusted to correspond to the C20 bogie including two motorized wheelsets. However, here no driving torque is applied to the wheelsets. Only the leading bogie in the car is used for the wear simulations. Both its wheelsets are modelled with flexible wheel axles. The trailing bogie is non-motorised and has rigid axles. The trailing bogie and the car are kept unmodified throughout all simulations. According to [23] the largest magnitude contact forces are generated at the leading bogie of the second car. The car load of the obtained vehicle is modified to adjust the leading bogie forces towards this case. Modifications in the vehicle model are isolated to the added weight of the car and the wheel axle flexibility.

The wheelset structural flexibility has important significance at frequencies above about 50 Hz and hence in the frequency range of interest in the current study. The wheelset was therefore modelled as flexible. The primary suspension effectively isolates the unsprung mass from the train components above the primary suspension at frequencies above about 20 Hz. Hence, excluding the wheelsets, all other train components are modelled as rigid. The final assembled model can be seen in Figure 3.4.

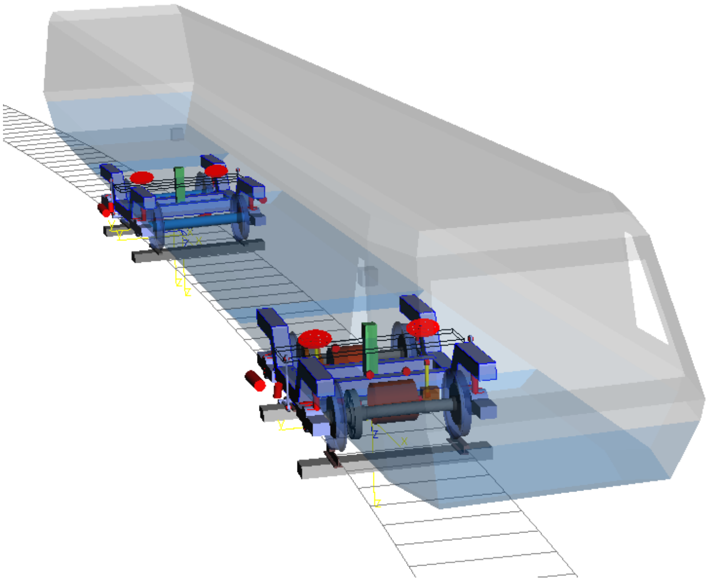

Figure 3.4: Simpack model mimicking one car of the C20 train.

3.2.2.1 Wheelset structural flexibility

The flexible wheel axle was imported to Simpack from the commercial software for finite element analysis Abaqus. In Simpack flexible bodies are represented by their eigenmodes and eigenvalues. Modal synthesis was performed in Abaqus. The FE-model of the wheelset includes solid brick elements for the axle and solid tetrahedral elements for the spur wheel. To enable the wheel axle connections (e.g. to wheels, axle boxes, etc.) in the subsequent Simpack simulations, so-called interface nodes are introduced. These nodes are created on the rotation axis of the wheelset and are rigidly connected to all selected nodes on the surface of the wheel axle, see Figure 3.5. This results in these surfaces being rigid, however, these surfaces are much smaller than the general dimensions of the axle. The interface nodes have six degrees of freedom compared to three for the solid element nodes. This is possible due to the multiple rigid connections to the surface nodes.

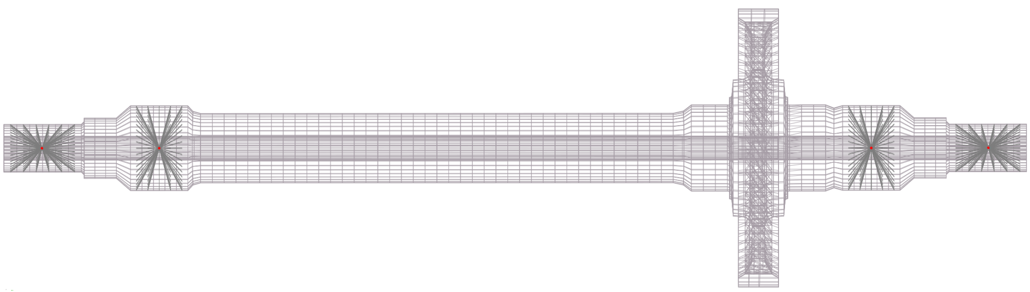

Figure 3.5: Illustration of axle interface nodes and connection to mesh.

Modal synthesis of the wheelset FE-model originally containing a total of 103 512 dofs was performed retaining the 70 lowest frequency eigenmodes. The wheels were modelled as rigid and added to the axle in Simpack using rigid connections to the corresponding interface nodes. In Simpack the wheel axles were the only components modelled as flexible. The primary suspension corresponds to a low-pass filter effectively isolating the high-frequency dynamics to the unsprung mass. This motivates the use of rigid bodies to model the bogie frame and the car. The properties of the assembled wheelset are presented in Table 3.1. Eigenmodes corresponding to the lowest seven eigenvalues calculated for free boundary conditions are shown in Figure 3.6. These are the modes used to account for the wheelset flexibility in the assembled vehicle model.

Table 3.1: Flexible wheelset properties and mode frequencies.

Mass, m	794 kg
Inertia around x, I_{xx}	374 kg/m^2
Inertia around y, I_{yy}	50 kg/m^2
Inertia around z, I_{zz}	374 kg/m^2
First antisymmetric torsion	79 Hz
First symmetric bending	95 Hz
First antisymmetric bending	225 Hz
Second symmetric bending	518 Hz
First symmetric torsion	570 Hz
First symmetric axial	605 Hz
Second antisymmetric bending	708 Hz

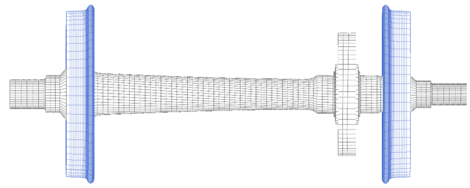

(a) 79 Hz

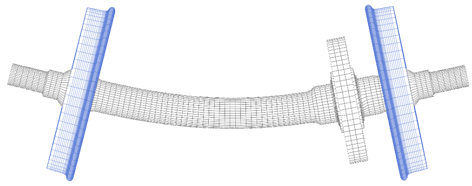

(b) 95 Hz

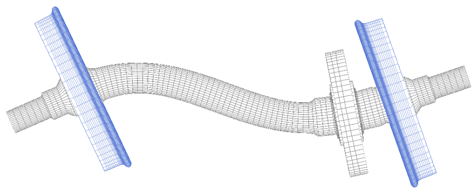

(c) 225 Hz

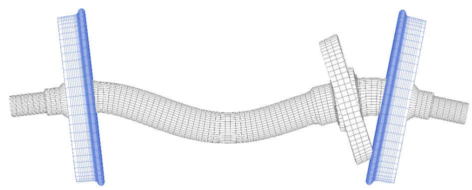

(d) 518 Hz

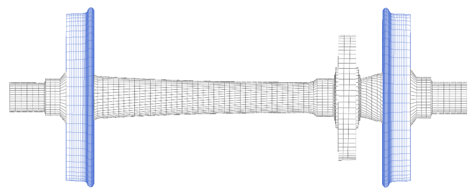

(e) 570 Hz

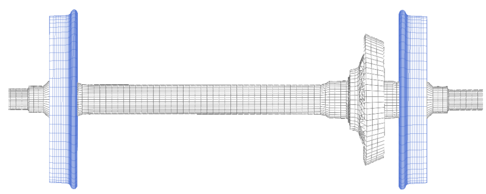

(f) 605 Hz

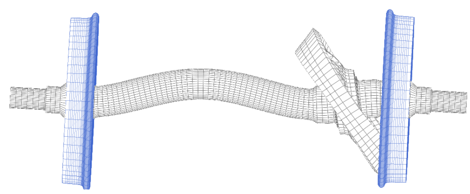

(g) 708 Hz

Figure 3.6: The lowest seven eigenmodes for the wheelset and their associated eigenfrequencies.

3.2.3 Wheel–rail contact

Simpack subjects the wheel–rail contact to several simplifications [21]. In solving the contact problem only the rail profile vertically below the wheelset rotation axis is used to describe the rail. This assumes a constant rail profile shape in the entire contact area. The number of contact points are determined from the intersection of the three-dimensional contact surfaces of the wheel and rail. The wheelset yaw angle is accounted for. The assumption of a constant rail profile throughout the wheel–rail contact area leads to an error in the estimated contact position in the longitudinal direction. This is because the displacement of the contact area towards the closest corrugation peak occurring for real cases of short wavelength corrugation is not captured. By a pure geometrical assessment it can be shown that a wavelength of 45 mm and amplitude of 0.1 mm will result in a maximum longitudinal shift of about 5.5 mm.

For modelling the wheel–rail contact in Simpack, the theory by Hertz and the algorithm FASTSIM are used in the normal and tangential directions, respectively. FASTSIM is an implementation of Kalker's steady-state simplified theory of rolling contact [24].

3.3 Contact post-processing in Matlab

As already has been discussed, the contact analysis in Simpack assumes a non-varying rail profile in the contact area, Hertzian normal contact and steady-state tangential contact. All these assumptions are often applicable in simulations of dynamic vehicle–track interaction. However, in calculations of wear they may introduce a significant error [10]. To achieve an accurate calculation of the rail wear the contact is re-evaluated in a post-processing step in Matlab. Taking the true three-dimensional contact geometries of the rail and wheel at positions resulting from the time integration of the vehicle-track system could possibly lead to large penetrations and consequently an overprediction of the contact forces. This is avoided by shifting the wheel vertical position until the resulting normal wheel–rail contact force corresponds to that obtained from Simpack.

To solve for the stresses and sliding in the wheel–rail contact, the same algorithm as used in [22] is applied. This is an implementation of Kalker's variational method. The contact problem is solved for a mesh with quadratic elements of side length 1 mm. In the post-processing step the contact problem is solved with a sampling frequency of 8320 Hz. This corresponds to the vehicle, with speed 30 km/h, traveling one element length. Given the wheel and rail contact geometries, and the normal force and creepages from the Simpack simulation, the post-processing step in Matlab provides a detailed contact estimation.

A representative set of re-evaluated contacts is illustrated in Figure 3.7. The longitudinal x-coordinate for each contact is based on the midpoint of the Hertzian contact evaluated by Simpack. Note that the geometric shift is captured in the re-evaluation.

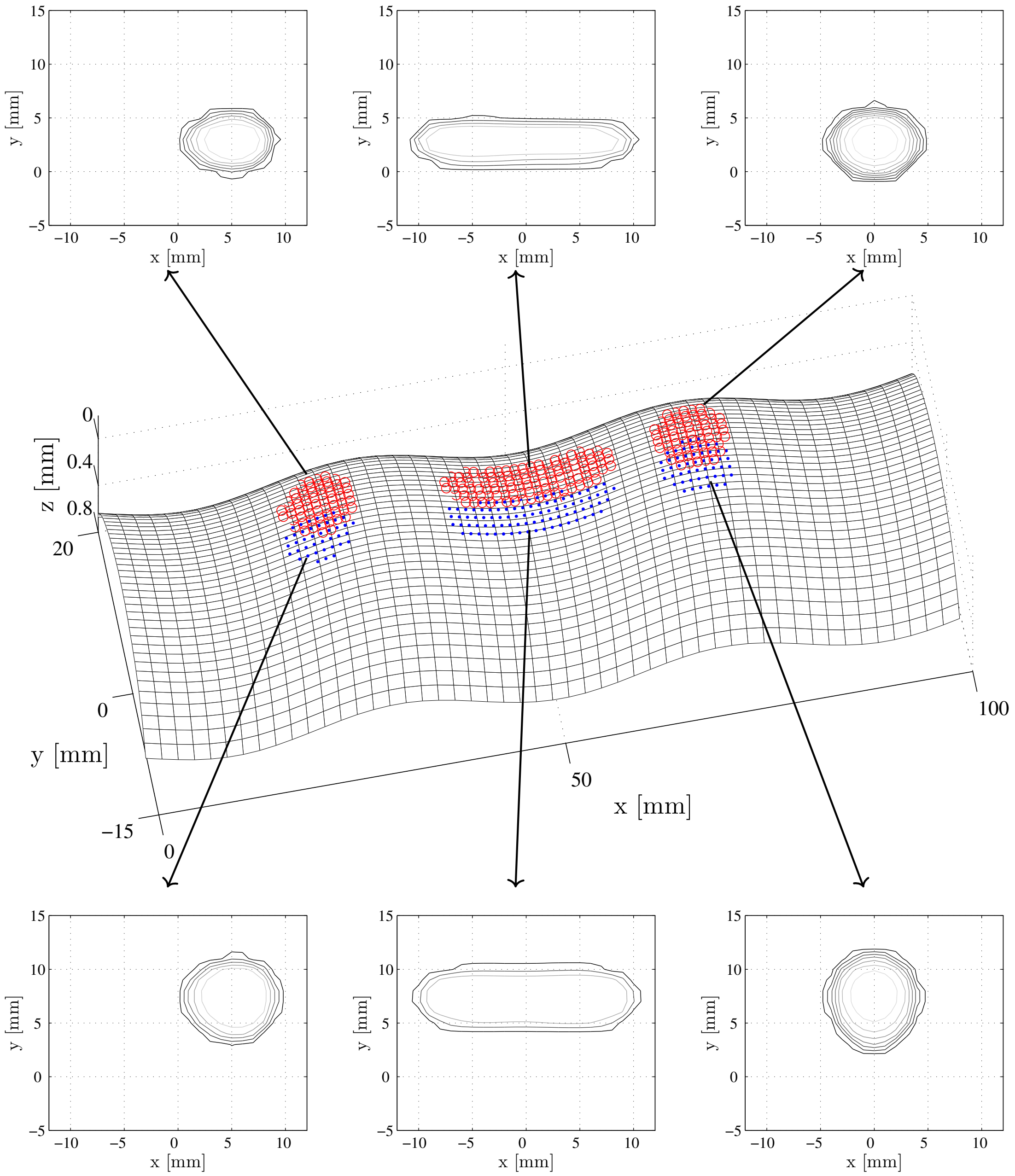

Figure 3.7: Wheels rolling on a single 40 mm wavelength rail irregularity with 0.1 mm amplitude. Contact location and normal contact pressure distribution for leading (blue dots) and trailing (red circles) wheelset, respectively. Vehicle speed 30 km/h, rail inclination 1:40, friction 0.6, curve raidus 120 m.

3.3.1 Updating of the rail surface irregularity

Archard's law is applied to calculate wear. The wear coefficient and material hardness were chosen as $k = 10^{-4}[-]$ and $H = 3.4 \times 10^{9}[\mathrm{N/m^2}]$ [18], respectively. The wear depth calculated at a specific time-step is mapped over to a mesh containing the accumulated wear for the complete rail and several train passages. The wear volume from a contact node is split up to its four closest neighbours on the rail mesh.

Using the notations in Figure 3.8b the contact node wear depth δz distributed to rail node wear depth Δz_1 is calculated as

$$\Delta z_1(\delta z) = \delta z \frac{axby}{\delta x \delta y} \frac{\Delta x \Delta y}{\delta x \delta y} \tag{3.1}$$

This guarantees that the wear volume is preserved. The resulting in-plane volume shift is small. A smooth contact wear will always result in a smooth rail wear distribution provided that the rail elements are larger than the contact elements.

From the rail mesh, rail profiles to be used in the simulations of dynamic vehicle–track interaction in Simpack are linearly interpolated.

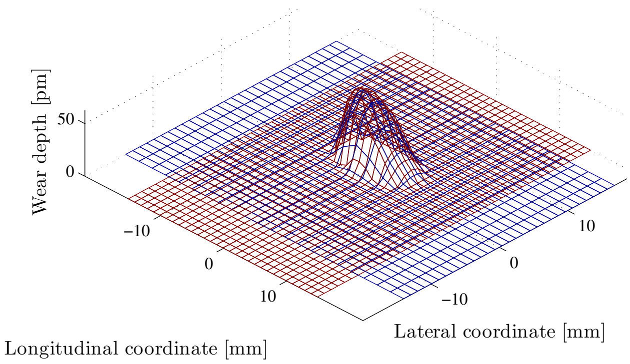

(a)

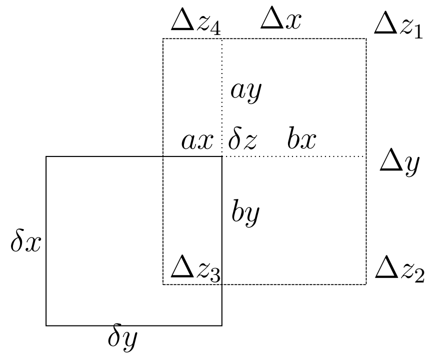

(b)

Figure 3.8: Illustration of wear depth mapped from contact mesh on to rail mesh. (a) Contact wear (quadratic elements) mapped to a section of the rail mesh (rectangular elements). (b) Contact and rail element.

3.4 Simulation of long-term roughness growth

For the possibility to predict long-term rail corrugation growth the simulation of a large number of train passes is required. The procedure used consists of three modules; (1) the simulation of dynamic vehicle-track interaction in Simpack, (2) the contact re-evaluation and (3) updating of the rail irregularity with respect to the generated wear. The method is summarized below.

Outline of steps performed in the main Matlab script.

1. Start by generating an initial rail geometry with a representative roughness, save this in a format that Simpack can read.
2. Call the Simpack solver and simulate one train passage.
3. Make a detailed re-evaluation of all contacts by using the results from the simulation and the rail geometry from step 1.
4. Evaluate the corresponding wear for each contact, assemble these and multiply with a number of train passes. Update the rail geometry by removing this quantity.
5. Return to step 2 until sufficiently many train passes have been simulated.

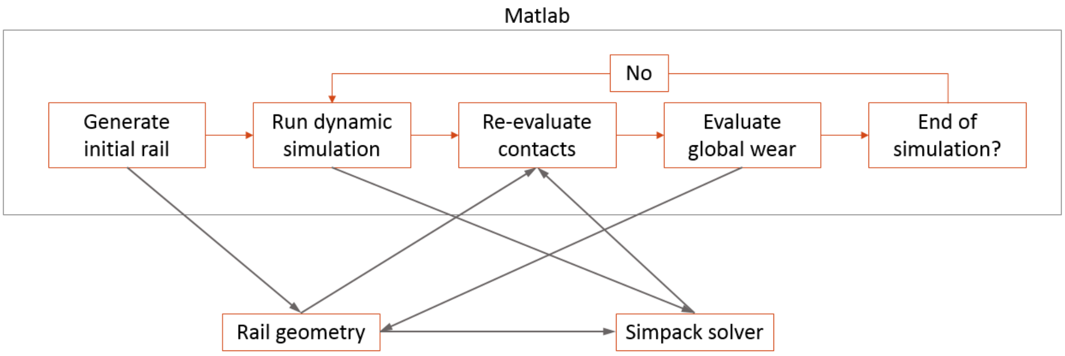

Figure 3.9: Outline of Matlab script.

To simulate a large number of train passages a multiplication factor of 2000 - 10 000 is used for the wear depth calculated for one train passage. Before the next simulation in Simpack, the rail surface geometry is updated with respect to the wear generated by previous train passes.
A graphic representation of the simulation scheme is seen in Figure 3.10.

3.4.1 Initial rail roughness

The initial rail irregularity influences the development of corrugation. In the proposed simulation procedure, three different options for the initial irregularity can be made. An arbitrary roughness can be set by providing a set of wavelengths and corresponding amplitudes. The second option is to simply provide the raw space domain roughness signal. This could for example be a measured signal from a recently ground rail. The third option is to set the roughness level according to the ISO 3095 limit. To do this the script developed in [25] was used. An option for inducing additional lateral irregularity with smooth longitudinal variation was also developed.

3.4.2 Simulation setup

Measures were taken in order to decrease the simulation time. By only calculating wear for a section of the circular curve where steady-state curving is obtained the

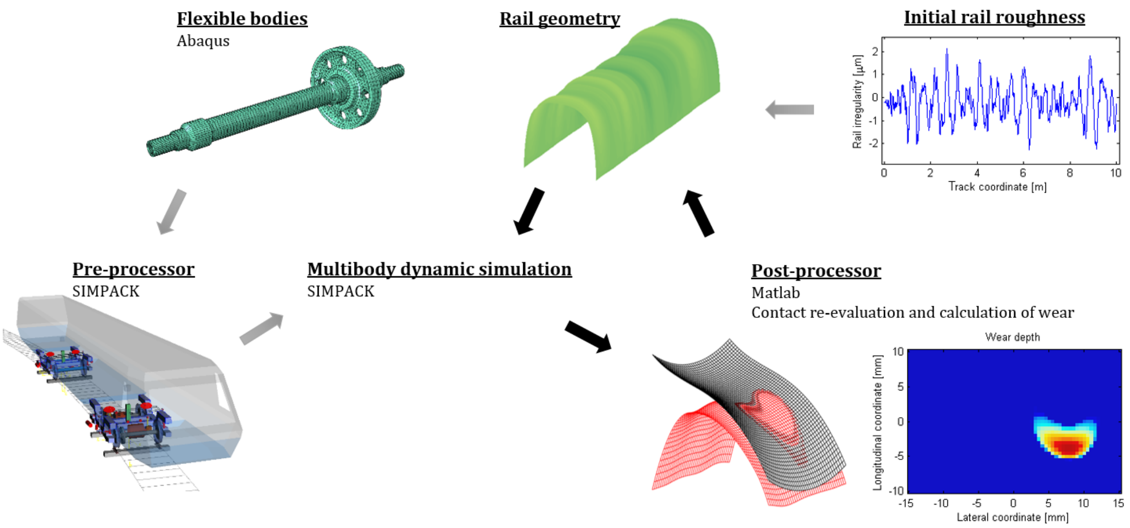

Figure 3.10: Illustration of iteration procedure used to simulate long-term corrugation growth.

running section could be reduced. It was found that the train had obtained a steady-state curving position at longitudinal coordinate 190 m. Hence wear was assessed starting at this coordinate. It is important to remark that if the operational parameters are changed (e.g. vehicle speed, friction coefficient, wheelset stiffness, etc.), the dynamic vehicle-track interaction needs to be re-simulated from the start on the tangent track.

Updating of the rail geometry with respect to corrugation is done over a 10 m long section from longitudinal coordinate 195 m to 205 m. The transition between the unworn rail at 190 m and the worn rail at 195 m is found to be sufficiently long in order to reduce transients, see Figure 3.11. A linear ramp up of the corrugation magnitude for the first 30 cm of the corrugated rail section is modelled.

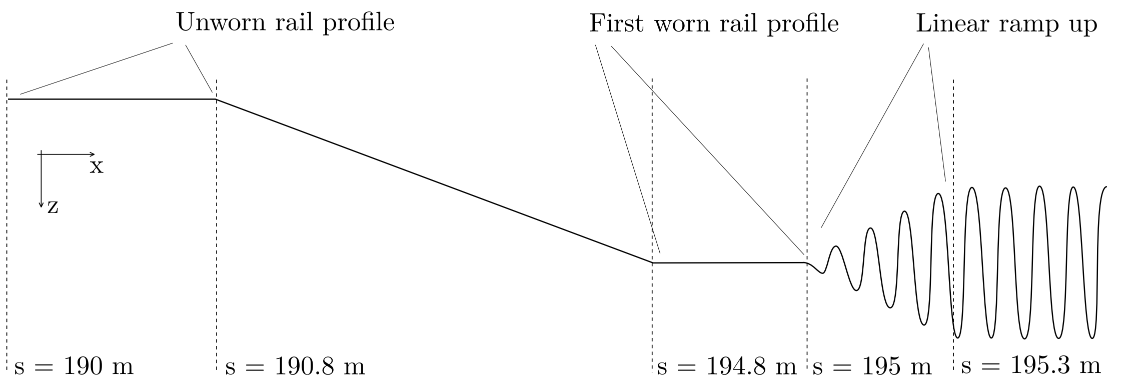

Figure 3.11: Transition between unworn rail and corrugated section for section of the rail.

4
Results

4.1 Measurements of rail roughness on the reference curve

Measurement of rail roughness was performed on the reference curve on the Stockholm metro approximately six months after grinding. Roughness was measured in three parallel lines with an APT - RSA equipment. Long wavelength track irregularities have not been considered. Spectral analysis of the measurement data shows presence of corrugation at several wavelengths. The largest levels are found at the approximate wavelengths of 5 cm and 10 cm, see Figure 4.1. Previous measurement campaigns on the same curve have shown similar results [1] with peaks in roughness level at wavelengths of about 5 cm and 8 cm. Moreover it was found that corrugation developed into a constant amplitude after about 300 days after grinding.

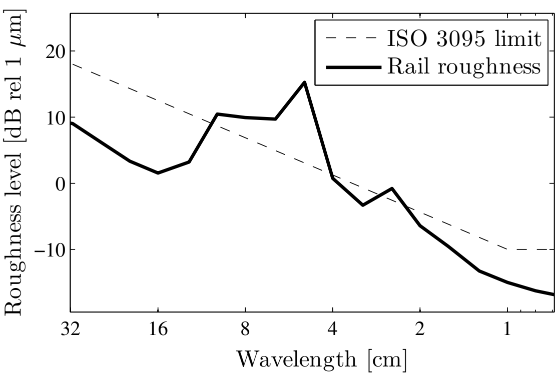

Figure 4.1: Rail roughness level in 1/3 octave bands measured on the low rail of the reference curve

4.2 Vehicle curving behaviour on the reference curve

The curving behaviour of the current vehicle model on a track with geometry in accordance with the reference curve is simulated. Results for the leading bogie obtained from Simpack at vehicle speed 30 km/h are shown. These results are directly obtained from the vehicle–track simulation.

4.2.1 Transient curving behaviour

In Figure 4.2 the normal and tangential wheel–rail contact forces for the leading bogie are presented. Results are shown from the tangent track until steady-state curving is achieved in the circular curve at approximate longitudinal coordinate 170 m. The transition curve starts and ends at longitudinal coordinates 100 m and 150 m, respectively. At approximate longitudinal track coordinate 110 m a flange contact is developed for the leading wheelset, see Figure 4.2. Note that the flange contact is much more severe if friction is increased, corresponding to a further displacement of the leading wheelset towards the high rail. Note also that the magnitudes of the forces are relatively similar for the two axles and that the influence of friction coefficient on normal forces is small.

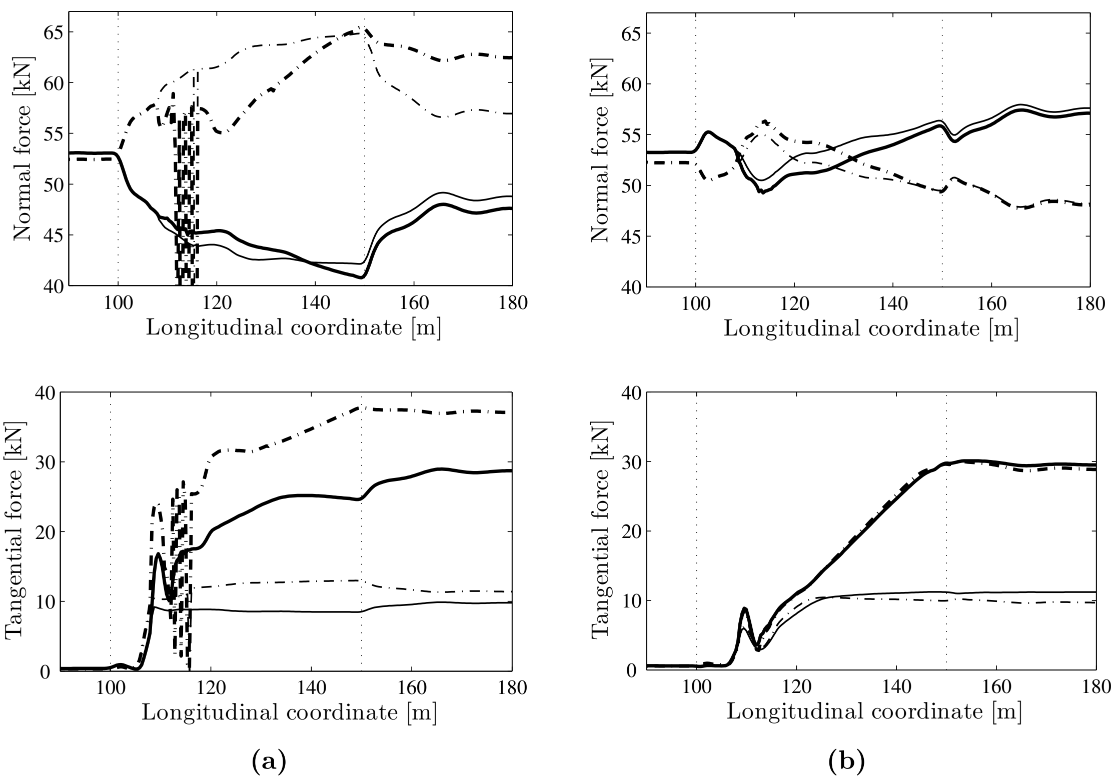

Figure 4.2: Normal and tangential wheel–rail contact forces, for leading (a) and trailing axle (b). Calculated for vehicle speed 30 km/h. (—) $\mu = 0.2$ low rail, (-·-) $\mu = 0.2$ high rail, (**—**) $\mu = 0.6$ low rail, (**-·-**) $\mu = 0.6$ high rail.

Figure 4.3 shows that the creepages for the leading wheelset on the low rail exceeds those obtained for the trailing wheelset. This suggests that the wear will have its largest contribution from the leading wheelset. It can also be seen that an increased friction will reduce longitudinal creepage and increase lateral creepage. The metallurgical study performed on the same rail in [25] showed plastic flow on the rail head mainly directed towards the field side. This suggests that the true friction coefficient is much closer to 0.6 than to 0.2 when wear and plastic flow is generated.

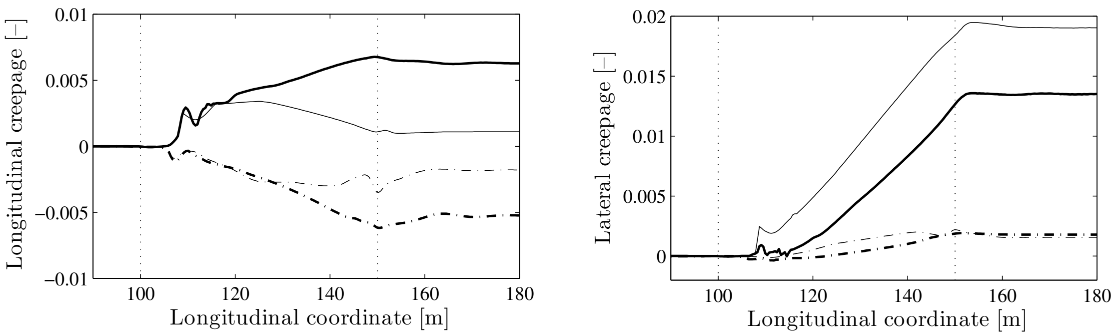

(a) **(b)**

Figure 4.3: Longitudinal (a) and lateral (b) creepages on the low rail for the leading and trailing wheelsets of the leading bogie. Directions are positive in the travelling direction, and towards the field side, respectively. Vehicle speed 30 km/h. (—) $\mu = 0.2$ leading axle, (-·-) $\mu = 0.2$ trailing axle, (**—**) $\mu = 0.6$ leading axle, (**-·-**) $\mu = 0.6$ trailing axle.

The lateral contact positions on the low rail are shown in Figure 4.4. For both levels of friction the contact position on the low rail for the leading wheelset is seen to occur on the rail crown. For friction coefficient 0.2 the trailing wheelset is displaced towards the low rail (not shown here) corresponding to a lateral contact position towards the rail gauge face. It is important to keep in mind that the lateral contact position has a strong non-linear dependence on the wheel–rail relative lateral shift.

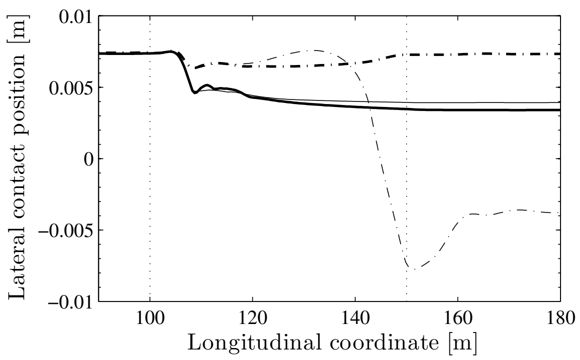

Figure 4.4: Lateral contact position on the low rail for the leading and trailing wheelset, respectively. Results are calculated for friction coefficient 0.2 and 0.6. Direction is positive towards the field side. Vehicle speed 30 km/h. (—) $\mu = 0.2$ leading axle, (-·-) $\mu = 0.2$ trailing axle, (**—**) $\mu = 0.6$ leading axle, (**-·-**) $\mu = 0.6$ trailing axle.

Yaw angles of both wheelsets and the frame of the leading bogie are presented in Figure 4.5. The leading wheelset has a large under-steering yaw angle whilst the trailing wheelset has an almost radial steering position. The bogie has about half as much under-steering as the leading wheelset. Lowering the friction increases the yaw angle of the leading wheelset and the bogie frame.

The yaw angle observed for the leading wheelset causes the large magnitude lateral creepage seen in Figure 4.3b. The lateral creepage caused by the large yaw angle of the leading wheelset creates a force acting on the wheelset directed outwards in the curve towards the high rail. This results in a rolling radius difference of the leading wheelset corresponding to a negative longitudinal creep on the high rail and a positive longitudinal creep on the low rail. As a result tangential creep forces are developed that strives to reduce the yaw angle of the wheelset. Limiting these forces by reducing the friction will therefore lead to an increase in yaw for the leading wheelset, as can be seen in Figure 4.5.

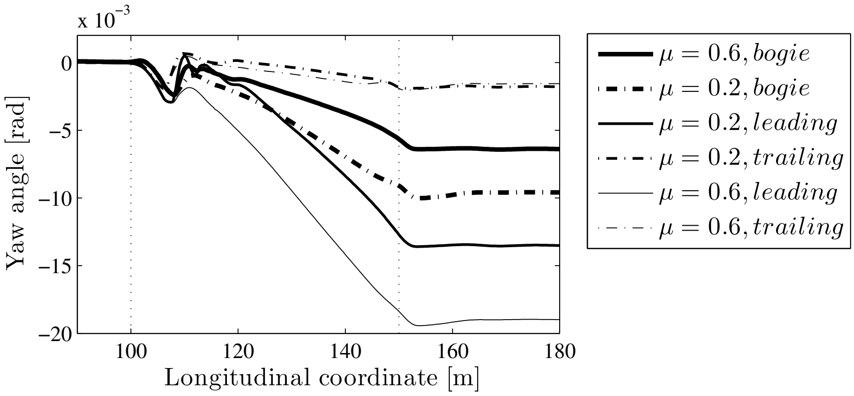

Figure 4.5: Yaw angles calculated for both wheelset and frame of the leading bogie. Friction coefficient 0.2 and 0.6 are used. The angle is defined positive around the z-axis, thus the bogie is in under-radial steering position. Vehicle speed 30 km/h.

4.2.2 Coupled vehicle–track eigenmodes

To illustrate the coupling between the vehicle and the track, the assembled system is analyzed in the frequency domain. The system is linearized in the steady-state curving situation. In the visualization all components except the leading wheelset and its track components are removed. The lowest frequency eigenmodes of the complete system which include a significant vibration at the low rail contact of the leading wheelset are assessed. Results calculated with rigid or flexible wheelsets including the seven lowest frequency eigenmodes are shown in Figure 4.6 and 4.7, respectively. Note that due to the choice of track model all track movements are in the xz-plane.

Figure 4.6 shows six eigenmodes calculated with the rigid wheelset model. The so called P2 resonance, where the wheelset, rails and sleeper vibrate in phase on the stiffness of the ballast occurs at about 50 Hz is not shown here. Figure 4.6a illustrates an eigenmode including a lateral vibration in opposite directions of the wheelset and sleeper. Eigenmodes in Figure 4.6b to 4.6d include a significant deformation of the rail pad and lateral, vertical and rotational vibration of the sleeper.

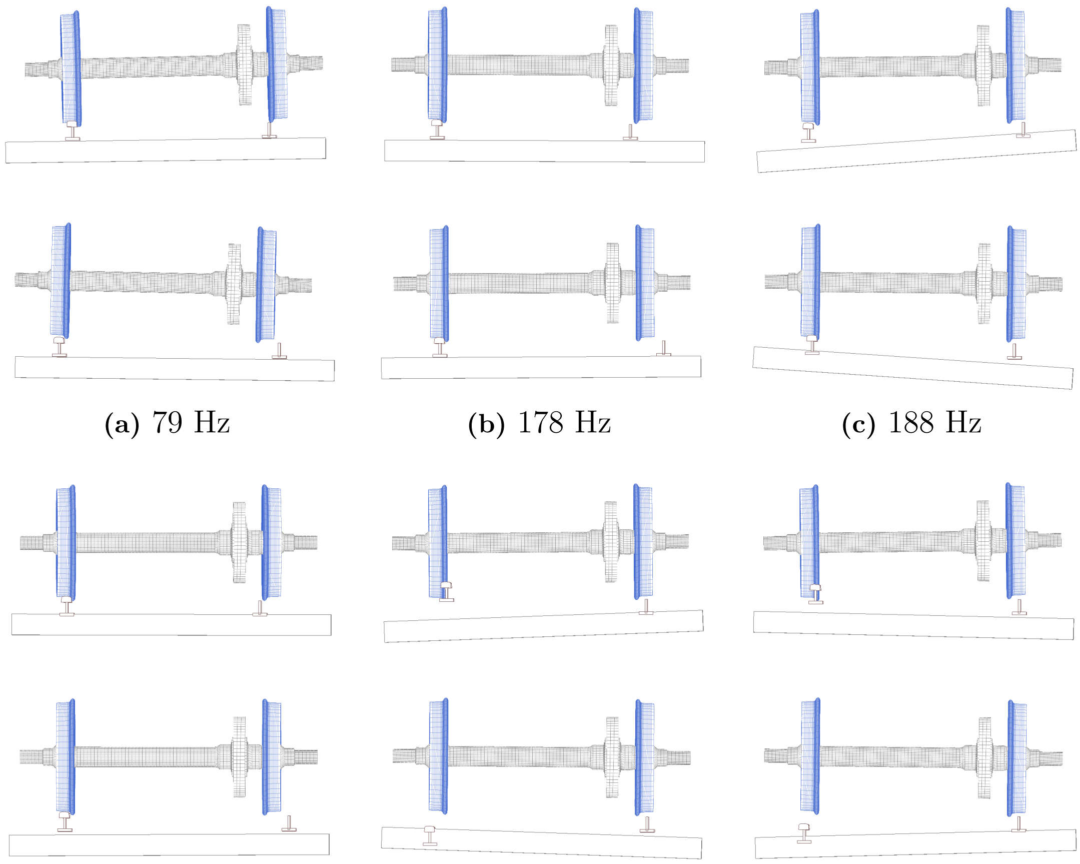

(a) 79 Hz (b) 178 Hz (c) 188 Hz

(d) 212 Hz (e) 490 Hz (f) 526 Hz

Figure 4.6: Coupled vehicle–track eigenmodes calculated for the leading wheelset of the leading bogie during steady-state curving. The wheelsets are modelled as rigid. Curve radius 120 m, vehicle speed 30 km/h. Eigenfrequencies associated with the six lowest frequency eigenmodes are outlined.

An analysis of the eigenmodes for the system with flexible wheelsets is performed. Eigenmodes associated with the eight lowest frequency eigenvalues, calculated for the leading wheelset of the leading bogie in steady-state curving, are shown in Figure 4.7. For an eigenfrequency of about 55 Hz, Figure 4.7a shows a coupled vibration corresponding to the P2 resonance in combination with the first symmetric bending eigenmode of the wheelset. The first symmetric bending eigenmode is also dominant for the eigenfrequency at 125 Hz, see Figure 4.7b. Eigenmodes in Figure 4.7c through 4.7e are similar to the results obtained with the rigid wheelset in the corresponding frequency range, but involves in addition a vibration of the wheelset in its first antisymmetric bending eigenmode. Eigenfrequencies for the free wheelset are found in Table 3.1.

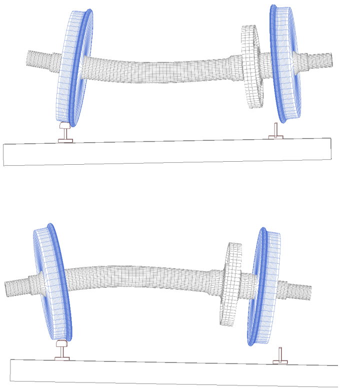

(a) 55 Hz

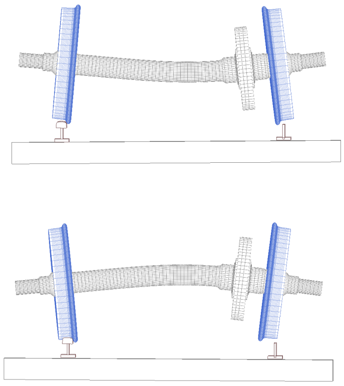

(b) 125 Hz

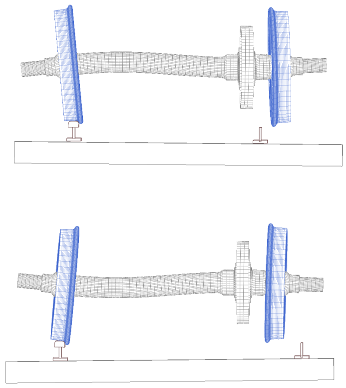

(c) 178 Hz

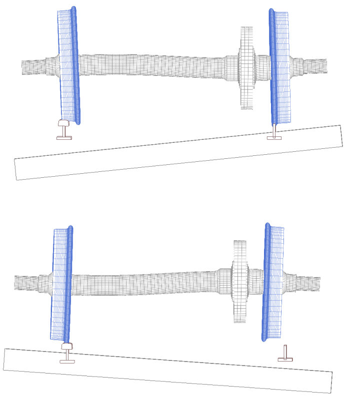

(d) 199 Hz

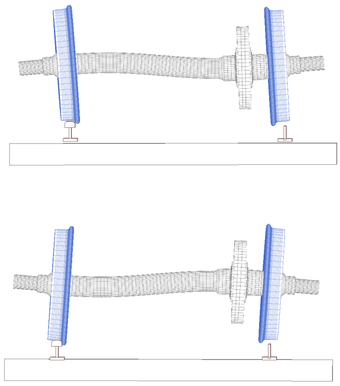

(e) 231 Hz

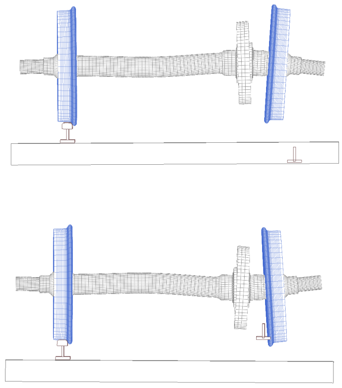

(f) 355 Hz

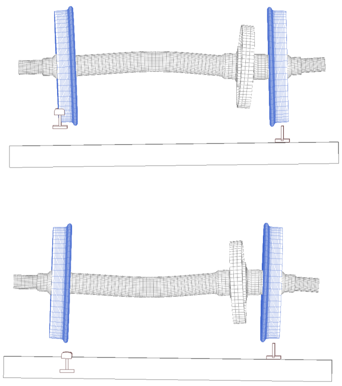

(g) 455 Hz

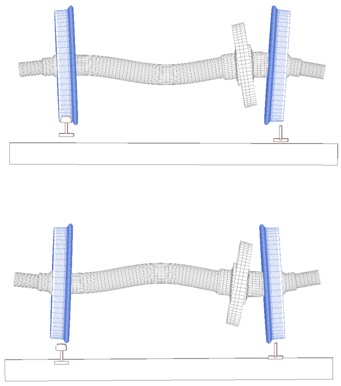

(h) 517 Hz

Figure 4.7: Coupled vehicle-track eigenmodes calculated for the leading wheelset of the leading bogie during steady-state curving. The wheelsets are modelled as flexible. Curve radius 120 m, vehicle speed 30 km/h. Eigenfrequencies associated with the six lowest frequency eigenmodes are outlined.

4.3 Prediction of corrugation growth

In the following, results from the post-processing performed in Matlab are discussed.

4.3.1 Verification of wheel–rail contact post-processing

The implementation of the post-processing step in Matlab is verified by comparing calculated contact pressures with those obtained in Simpack. Due to the large variation in lateral contact positions at different locations along the track, low rail contact of the trailing wheelset and friction coefficient 0.2 is considered, see Figure 4.4. Results obtained at longitudinal coordinates 80 m (tangent track), 125 m (transition curve) and 180 m (circular curve), are shown in Figure 4.8 through 4.10, respectively. The corresponding calculated wear depth is also shown.

Due to the vanishing creepages on the tangent track, see Figure 4.3, the generated wear is negligible, see Figure 4.8b. As expected the wear calculated for the other cases is concentrated in the slip region in the trailing edge of the contact patch, see Figure 4.9b and 4.10b.

For the non-conformal contacts in Figure 4.8a and 4.9a Simpack and Matlab yield similar contact pressure distributions. The normal contact pressure distributions are close to parabolic. In the circular curve the low rail contact of the trailing wheelset becomes close to conformal. For this non-Hertzian contact condition the difference between the models is significant, see Figure 4.10a.

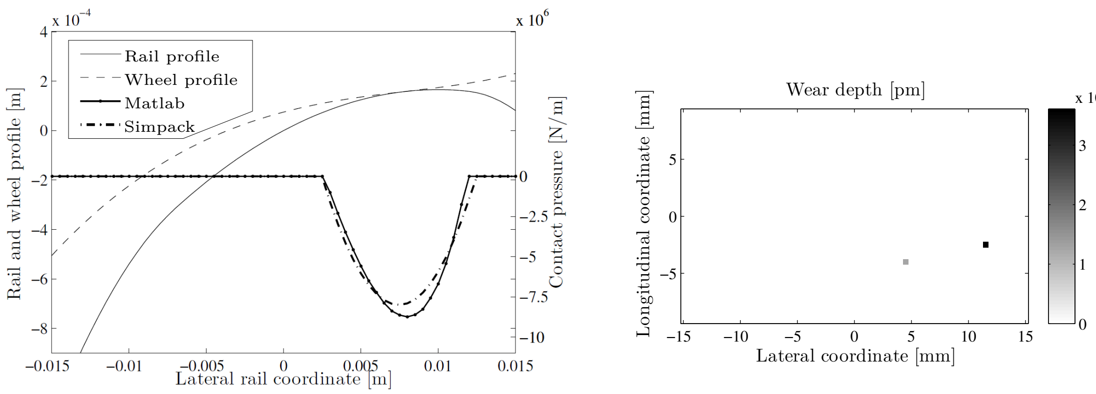

(a) (b)

Figure 4.8: Comparison of results calculated in Simpack and those obtained in the post-processing step in Matlab, for the low rail contact of the trailing wheelset. Longitudinal coordinate 80 m (tangent track), friction coefficient 0.2 and vehicle speed 30 km/h. (a) Contact pressure integrated longitudinally. The local wheel and rail profiles are outlined. (b) Calculated wear depth.

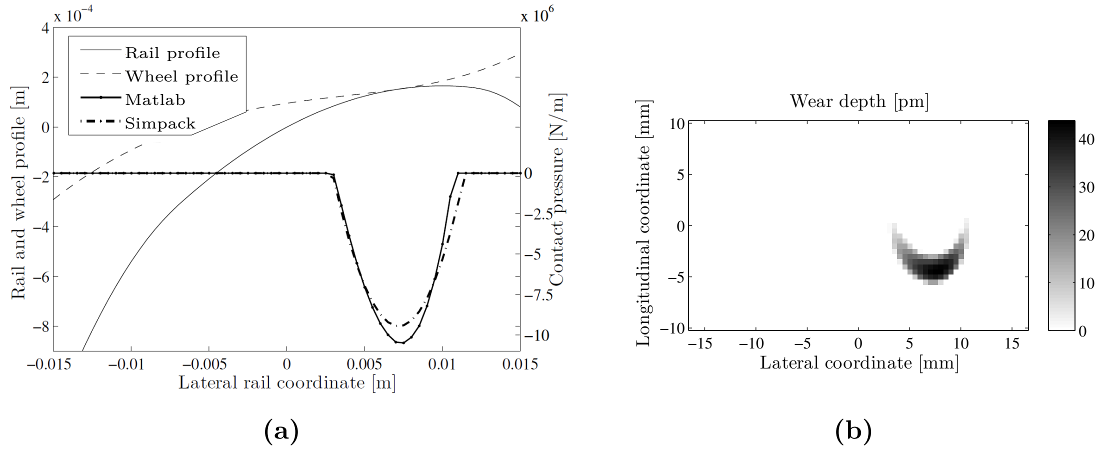

Figure 4.9: Comparison of results calculated in Simpack and those obtained in the post-processing step in Matlab, for the low rail contact of the trailing wheelset. Longitudinal coordinate 125 m (transition curve), friction coefficient 0.2 and vehicle speed 30 km/h. (a) Contact pressure integrated longitudinally. The local wheel and rail profiles are outlined. (b) Calculated wear depth.

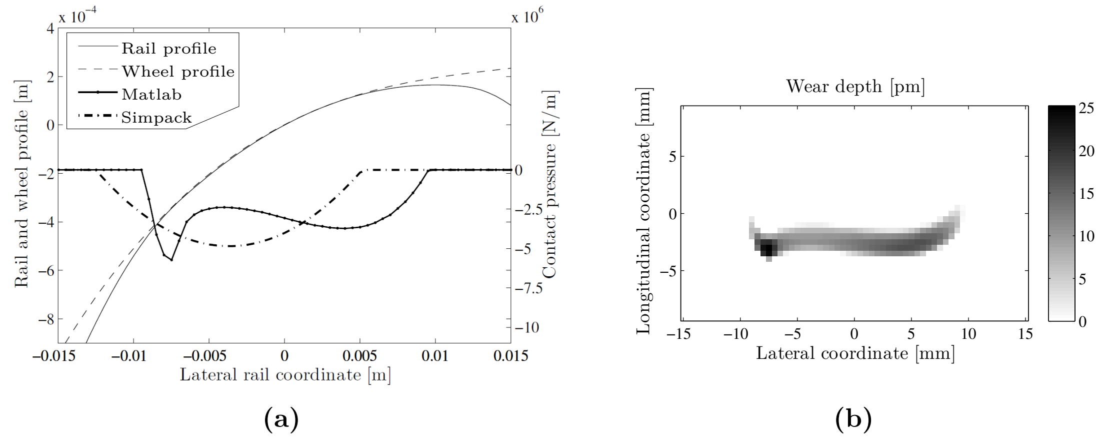

Figure 4.10: Comparison of results calculated in Simpack and those obtained in the post-processing step in Matlab, for the low rail contact of the trailing wheelset. Longitudinal coordinate 180 m (circular curve), friction coefficient 0.2 and vehicle speed 30 km/h. (a) Contact pressure integrated longitudinally. The local wheel and rail profiles are outlined. (b) Calculated wear depth.

4.3.2 Wavelength fixing mechanisms

By comparing the calculated wear depth with the initial rail irregularity, an indication about which irregularity wavelengths that may be promoted over time is given. An important remark is that the system is non-linear and hence the generated wear depends on the current irregularity magnitudes. This issue is discussed in the next Section where results for long-term roughness growth are shown. In this Section the initial rail irregularity is taken in accordance with the ISO3095 standard. Irregularity wavelengths in the range from 2 cm to 64 cm are included. The same realization of the initial rail irregularity is used for all simulations presented in the following.

To investigate at which wavelengths the vehicle–track system promotes corrugation growth, the complex transfer function, $\bar{H}$, between the initial rail irregularity, $\bar{R}$, and the predicted wear depth, $\Delta\bar{Z}$, is calculated. The frequency contents of the rail irregularity is obtained using a discrete Fourier transform. Notations used are taken from [25].

$$\bar{H} = \frac{\Delta\bar{Z}}{\bar{R}} \tag{4.1}$$

The magnitude of the transfer function, $\bar{H}$, calculated for the low rail contacts of the leading bogie in the circular curve is presented in Figure 4.11. The case of steady-state curving at vehicle speed 30 km/h and friction coefficient 0.6 is considered. The amount of wear generated by the leading wheelset exceeds that of the trailing wheelset by approximately ten times. The transfer function magnitude calculated for the leading wheelset shows distinct peaks at approximate wavelengths 4.5 cm and 7 cm. These wavelengths are similar to the wavelengths observed on the reference curve of the Stockholm metro, see Section 4.1. For the current vehicle speed and the wavelength of 7 cm, the eigenmode at the corresponding eigenfrequency is presented in Figure 4.7b. For the wavelength of 4.5 cm, the eigenmodes at the corresponding eigenfrequency are presented in Figure 4.7c to 4.7e. The increased magnitude of the transfer function noted at the wavelength about 17 cm coincides with the P2 resonance, see Figure 4.7a. This corrugation wavelength is not represented in the measurement data from the reference curve and might be due to insufficient ballast damping or excitation from the initiation of the rail irregularities.

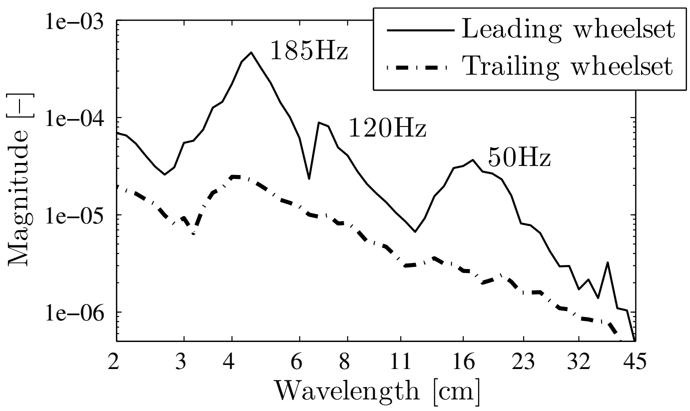

Figure 4.11: Magnitude of the transfer function between the initial rail irregularity and the wear depth calculated for both wheelsets of the leading bogie. Results calculated for flexible wheelsets given in 1/12 octave bands. Curve radius 120 m, vehicle speed 30 km/h and friction coefficient 0.6.

4.3.2.1 Wheelset structural flexibility

The cause of the distinct peaks seen in Figure 4.11 is investigated by varying selected model parameters. In Figure 4.12, results calculated accounting for wheelset structural flexibility are compared with those obtained for rigid wheelsets. Again the magnitude of the transfer function between the initial rail irregularity and the calculated wear depth is used. The wheelset structural flexibility is seen to have a significant influence on the magnitudes of the transfer function. It also leads to more distinct peaks in the transfer functions.

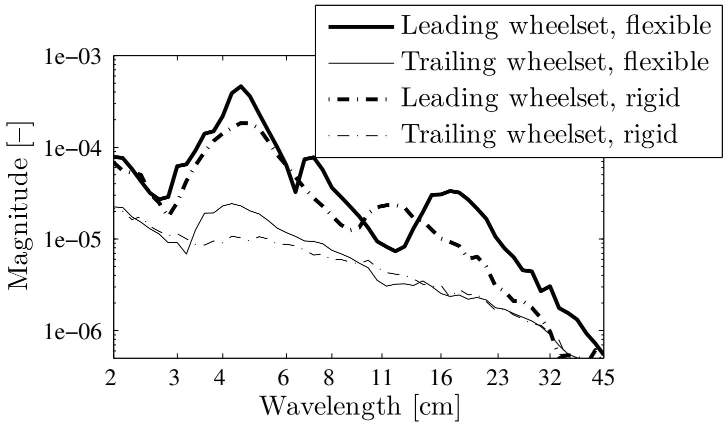

Figure 4.12: Magnitude of the transfer function between the initial rail irregularity and the wear depth calculated for both wheelsets of the leading bogie. Comparison of results calculated for flexible and rigid wheelsets given in 1/12 octave bands. Curve radius 120 m, vehicle speed 30 km/h and friction coefficient 0.6.

As observed in Figure 4.13, growth of corrugation at distinct wavelengths is also predicted for the case of the leading wheelset modelled as rigid. Here the wavelengths correspond to frequencies 70 Hz and 185 Hz. The peak in transfer function magnitude at 185 Hz may be related to the eigenmodes illustrated in Figure 4.6b through 4.6d, keeping in mind the poorly damped peak in the lateral receptance of the track in the same frequency range, see Figure 3.3b. For the flexible wheelset this also involves a significant vibration of the wheelset in its first antisymmetric bending eigenmode. The peak in transfer function magnitude calculated for the rigid wheelset at around 12 cm might be a combination of the P2 resonance and the eigenmode illustrated in Figure 4.6a.

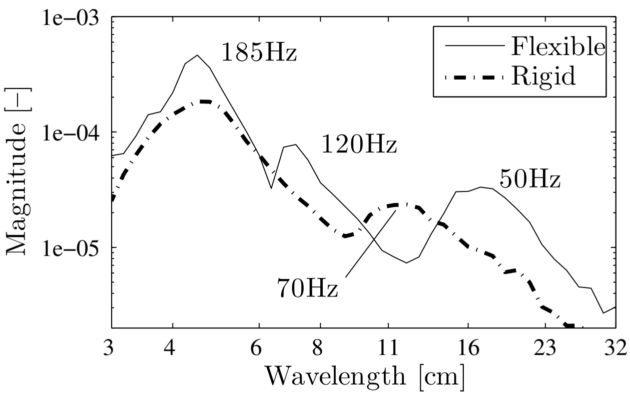

Figure 4.13: Magnitude of the transfer function between the initial rail irregularity and the wear depth calculated for the leading wheelset. Comparison of results calculated for flexible and rigid wheelsets given in 1/12 octave bands. Curve radius 120 m, vehicle speed 30 km/h and friction coefficient 0.6.

4.3.2.2 Friction dependence

One mitigation action for rail corrugation is the application of a friction modifier on the top of the rail. In Figures 4.14 and 4.15, the magnitude of the transfer function between the initial rail irregularity and the calculated wear depth, calculated for the low rail contacts of the leading bogie for different values of the wheel–rail friction, are shown. The wear coefficient is kept constant for all values of wheel–rail friction. The level of friction is seen to have a significant non-linear effect on the transfer function magnitudes. By reducing the friction coefficient the peaks in transfer function magnitudes at 50 Hz and 120 Hz are reduced whereas the one at 185 Hz seems more or less unaffected. Keep in mind that the wear coefficient, which has been kept constant throughout these simulations, has a friction dependence. The magnitudes for lower frictions can therefore be expected to be lower.

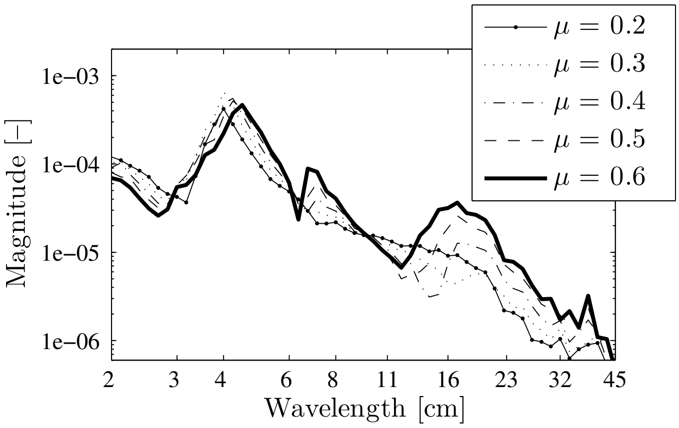

Figure 4.14: Friction dependent magnitude of the transfer function between the initial rail irregularity and the wear depth calculated for the leading wheelset. Results given in 1/12 octave bands. Curve radius 120 m and vehicle speed 30 km/h. Wheelset structural flexibility accounted for.

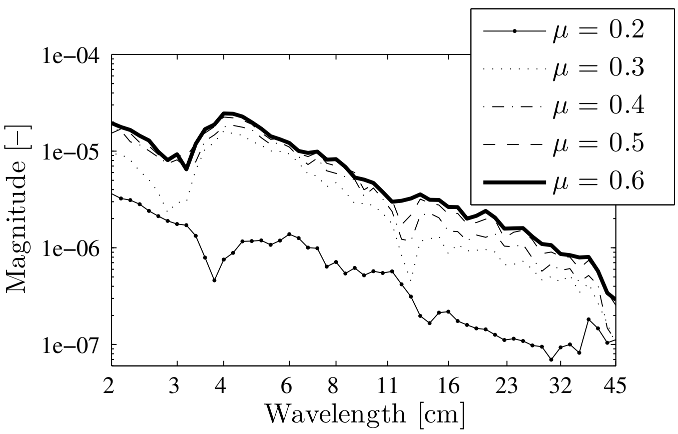

Figure 4.15: Friction dependent magnitude of the transfer function between the initial rail irregularity and the wear depth calculated for the trailing wheelset. Results given in 1/12 octave bands. Curve radius 120 m and vehicle speed 30 km/h. Wheelset structural flexibility accounted for.

4.3.3 Prediction of long-term corrugation growth

The development of long-term corrugation is predicted. The initial rail roughness is modelled in accordance with the ISO 3095 limit. 40 000 train passes are accounted for, corresponding to a total of 20 iteration steps in the proposed simulation procedure. Steady-state curving of the leading wheelset on the reference curve at vehicle speed 30 km/h and friction coefficient 0.6 is considered. Only wear generation from the leading bogie is accounted for.

Figure 4.16a shows a cut-out of the rail irregularity development. It is noticed that the final rail irregularity includes a dominant wavelength of approximately 4 cm. While increasing in magnitude, the corrugation formation at this wavelengths is also noticed to translate backwards with respect to the travelling direction of the vehicle. Spectra of the final and initial rail irregularity are compared in Figure 4.16b.

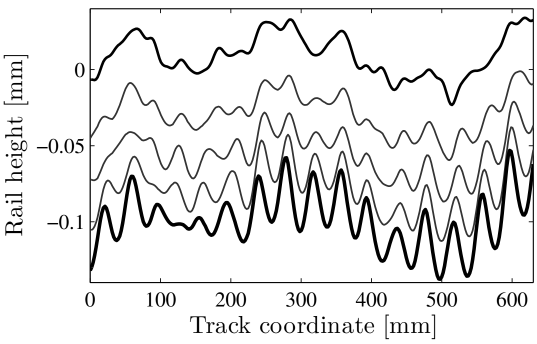

(a)

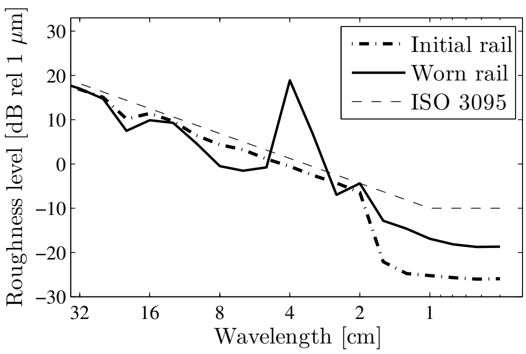

(b)

Figure 4.16: (a) Corrugation development predicted for 40 000 vehicle passages corresponding to 20 iteration steps in the simulation procedure. Resulting roughness after 0, 5, 10, 15 and 20 iterations. Steady-state curving on the reference curve at vehicle speed 30 km/h and friction coefficient 0.6. (b) Spectra of the rail irregularity predicted after 40 000 train passages and the initial rail irregularity presented in 1/3 octave bands.

5

Conclusions

A model able to predict long-term roughness growth on small radius curves has been developed and verified towards observations on a reference curve exposed to severe corrugation growth on the Stockholm metro. The proposed simulation procedure combines the robustness and versatility of the commercial multibody dynamics software Simpack, with an in-house model for calculation of the accumulated wear accounting for non-Hertzian and non-steady wheel–rail contact and Archard's law for sliding wear. The calculation of accumulated wear is based on the three-dimensional contact geometry of the wheel and rail.

The amount of wear generated by the leading wheelsets of passing bogies exceeds that of the trailing wheelsets. In addition the magnitude of the complex transfer function between the initial rail irregularity and the calculated wear depth calculated for the leading wheelset shows peaks at approximate wavelengths 4.5 cm and 7 cm. Possible wavelength-fixing mechanisms are investigated by eigenvalue analysis performed on the vehicle-track system linearized with respect to steady-state curving conditions. The corrugation wavelengths are associated with coupled vehicle-track vibrations including the first symmetric and first antisymmetric bending eigenmodes of the leading wheelset in passing bogies. These vibrations are exited by the wheelset yaw-angles and the resulting lateral wheel–rail contact forces with large magnitudes.

5.1 Error sources

The rail section that is updated with respect to the calculated wear is introduced by successively increasing the roughness magnitude over a total distance of 30 cm. The excitation of the P2 resonance might be possible to reduce by extending this section. Additional unwanted excitation may originate from the slope discontinuities at the start and end of the 4 m long linear ramp from the nominal to the worn rail profile.

The mass of the axle boxes and the sprocket housing are currently not modelled. This may lead to an over-estimation of the wheelset eigenfrequencies and could partly explain the predicted corrugation wavelengths in Figure 4.16b being shorter than those found in measurement data, see Figure 4.1.

Some other aspects whose influence have not been investigated are; the driving torque applied on the wheel axle sprocket, simplifications in the vehicle and track model, the true initial rail geometry and the variation of vehicle speeds.

5.2 Suggestions for future work

The developed model can be used to deepen the understanding of the complex mechanisms that promote corrugation growth. The proposed simulation procedure is not limited to the special type of "rutting corrugation", but is generally applicable presumeing that the structural flexibility of the train and track is accounted for in the studied frequency range.
Having a verified prediction model for corrugation growth enables an efficient search for mitigation measures or even actions to eliminate the problem. Examples of future studies suggested by the author are to investigate the possibility to use mixed traffic conditions (prescribed vehicle speed, axle load, train types, wheel and rail profiles, etc.) as a measure to prevent corrugation growth. Another possible use of the model is for the planning of maintenance intervals. Implementing a general purpose optimization algorithm in combination with the proposed model constitutes another possibility. Such an algorithm could optimize several parameters simultaneously towards a combination of objectives. Examples of optimization parameters are wheel and rail profiles, vehicle speed distribution, etc. In addition to quantities related to corrugation, the objective function could assess also for example passenger comfort. It is however important to consider the computational time for such an optimization. Some suitable algorithms can be found in the excellent work of Wahde [26].
The proposed model for prediction of long-term corrugation growth is readily able to use in combination with other vehicle models or other track geometries. Moreover it can easily be modified to account for wear generated by more wheelsets.
To better capture the real-world conditions, the author suggests to perform predictions of corrugation accounting for the statistical variance of input parameters such as vehicle speed, axle load, friction coefficient, etc. In addition measured wheel and rail profiles should be used.
The contact re-evaluation performed in the Matlab post-processing takes up a vast majority of the computational time. Each simulated train passage requires the worn rail from the previous run. This demands that the simulations are run in succession. Assuming, as has been done in the model, that the rail changes insignificantly for each train passage, the re-evaluation of rail–wheel contacts for different rail–wheel pairs are independent. This enables contacts from several rail–wheel pairs to be calculated simultaneously using parallel computing, reducing the simulation time to a fraction. Assuming steady-state rail–wheel contact enables parallel computing for all contacts of one rail–wheel pair.
The proposed simulation procedure includes a detailed model for dynamic vehicle-track interaction and a state-of-the-art post-processing calculation of wear. The possibility of reducing the complexity of the post-processing step by implementing a less detailed wheel–rail contact model is also part of future work. The present model could be used as a reference for validation.

Bibliography

[1] P.T. Torstensson, Rail Corrugation Growth on Curves. PhD thesis, Department of Applied Mechanics, Chalmers University of Technology, Göteborg, Sweden (2012)

[2] K. Knothe, A. Groß-Thebing, Short wavelength rail corrugation and non-steady-state contact mechanics, *Vehicle System Dynamics* **46** (2008) pp. 49–66

[3] N. Chaar, Wheelset Structural Flexibility and Track Flexibility in Vehicle-Track Dynamic Interaction. PhD thesis, Department of Aeronautical and Vehicle Engineering, Royal Institute of Technology (KTH), Stockholm, Sweden (2007)

[4] E. Andersson, M. Berg, S. Stichel, Rail Vehicle Dynamics, (KTH 2007)

[5] C. Esveld, Modern Railway Track (TUDelft 2001), *MRT-Productions*

[6] S.L. Grassie, R.W. Gregory, D. Harrison, K.L. Johnson, The dynamic response of railway track to high frequency vertical excitation, *Journal Mechanical Engineering Science* **24** (1982), pp. 77-90.

[7] S.L. Grassie, R.W. Gregory, K.L. Johnson, The dynamic response of railway track to high frequency lateral excitation, *Journal Mechanical Engineering Science* **24** (1982), pp. 91-95.

[8] R.A. Clark, P.A. Dean, J.A. Elkins, S.G. Newton, An investigation into the dynamic effects of railway vehicles runing on corrugated rails, *Journal Mechanical Engineering Science* **24** (1982), pp. 65-76.

[9] K.L. Johnson: Contact mechanics, Cambridge University Press, 1985. ISBN 0-521-25576-7. (Hertzian theory)

[10] M.S. Sichani, On Efficient Modelling of Wheel-Rail Contact in Vehicle Dynamic Simulation, PhD thesis, Department of Aeronautical and Vehicle Engineering, Royal Institute of Technology (KTH), Stockholm, Sweden (2016)

[11] F.W. Carter, On the action of a locomotive driving wheel, *Proceedings Royal Society* Series A, **112** (1926) pp. 151-157

[12] M.J. Boussinesq, Application des potentiels, *Gauthier-Villars*, Paris (1885)

[13] V. Cerruti, Mem. fis. mat. *Accademia dei Lincei*, Roma (1882)

[14] H. Hertz, Über die Berührung fester elastischer Körper, Journal für die reine und angewandte Mathematik 92, (1881) pp. 156-171

[15] J.J. Kalker, Three-dimensional elastic bodies in rolling contact, *Kluwer Academic Publishers, Dordrecht, Boston, London*, (1990)

[16] J.F. Archard, Elastic deformation and the laws of friction, *Proceedings of the Royal Society, Serial A*, **243** (1957) pp. 190–205

[17] T. Reye, Zur theorie der Zapfenreibung. Der Civilingenieur, 1860: pp. 235-255

[18] T. Jendel, Prediction of wheel profile wear-comparison with field measurements, *Wear* **253** (2002) pp. 89-99

[19] S.L. Grassie, J. Kalousek, Rail corrugation: characteristics, causes, and treatments. *Proceedings of the Institution of Mechanical Engineers, Part F: Journal of Rail and Rapid Transit*, **207** (1993) 75-68

[20] P.T. Torstensson, J.C.O. Nielsen, Monitoring of rail corrugation growth due to irregular wear on a railway metro curve, *Wear* **267** (2009) pp. 556-561

[21] Simpack manual, Simpack 9.9.1

[22] P.T. Torstensson, A. Pieringer, J.C.O. Nielsen, Simulation of rail roughness growth on small radius curves using a non-Hertzian and non-steady wheel–rail contact model, *Wear* **315** (2014) pp. 241-253

[23] Peter T. Torstensson, Jens C.O. Nielsen, Simulation of dynamics vehicle–track interaction on small radius curves, *Vehicle System Dynamics* **Vol. 49, No 11** (2011) pp. 1711-1732

[24] J.J. Kalker, A fast algorithm for the simplified theory of rolling contact, *Vehicle System Dynamics* **11** (1982) pp. 1-13

[25] P.T. Torstensson, M. Schilke, Rail corrugation growth on small radius curves – Measurements and validation of a numerical prediction model, *Wear* **303** (2013) pp. 381-396

[26] M. Wahde, Biologically Inspired Optimization Methods, Chalmers University of Technology, Sweden, *WIT Press*